UNIVERSITY OF CALIFORNIA

Los Angeles

Nanoscale Surface Photoreactions

A thesis submitted in partial satisfaction

of the requirements for the degree Master of Science in

Materials Science and Engineering

By

Garrett Austin Wadsworth

2014

ABSTRACT OF THE THESIS

Nanoscale Surface Photoreactions

By

Garrett Austin Wadsworth

Master of Science in Materials Science and Engineering

University of California, Los Angeles, 2014

Professor Paul S. Weiss, Chair

Subnanometer-scale properties of molecules and materials have become extremely important to the development of nanoscale and molecular electronics devices, including advanced biological and chemical sensors. The energies (*i.e.*, wavelengths) at which the LSPRs of individual nanoparticles are excited varies depending on their size, thickness, and shape, all of which can be controlled synthetically. Photon-coupled scanning tunneling microscopy uses a total internal reflection scheme to couple light into a tunneling junction, generating this specific LSPR in individual Au and Ag nanoprisms. By controlling and coupling this specific excitation to molecular assemblies, the effective photoreactivities and photoconductances of organic molecules can be measured and manipulated. Nanoparticle synthesis methods were developed to produce nanoprisms with appropriate dimensions and homogeneity. Functionalization of the sample surface using alkanedithiols and p-terphenyl-4,4”-dithiol enabled the adsorption

dispersion of nanoprisms onto substrates with high density yet minimal stacking. Insertion into self-assembled monolayers was used to arrange single molecules on Au{111} and Ag{111} nanoprisms for selective surface plasmonic enhancement. Scanning tunneling microscopy measurements were collected for molecules adsorbed on the dispersed nanoprisms. Photon STM will be used to monitor the photoactivities of molecules on these substrates, such as photocurrent, photoconductance, and photoreaction.

The thesis of Garrett Austin Wadsworth is approved.

Bruce S. Dunn

Yang Yang

Paul S. Weiss, Committee Chair

University of California, Los Angeles

2014

Table of Contents

List of Acronyms

AFM	Atomic force microscopy
APTES	(3-Aminopropyl)triethoxysilane
CTAB	Tetraurochlorate hexadecyltrimethylammoniumbromide
FF	Fill factor
I_T	Tunneling current
LSPR	Local surface plasmon resonance
OPV	Organic photovoltaic device
Photon STM	Photon-coupled scanning tunneling microscopy
PVD	Physical vapor deposition
RIU	Reflective index unit
SAM	Self-assembled monolayer
SEM	Scanning electron microscopy
SERS	Surface enhanced Raman spectroscopy
SPM	Surface probe microscopy
SPR	Surface plasmon resonance
SPW	Surface plasmon wave
STM	Scanning tunneling microscopy
TEM	Transmission electron microscopy
TPDT	p-Terphenyl-4,4”-dithiol
V_S	Sample bias
XPS	X-ray photoelectron spectroscopy

List of Figures

Acknowledgments

I would like to express my sincere gratitude to my advisor Prof. Paul Weiss for the continuous support of my study and research, for his patience, motivation, enthusiasm, and immense knowledge. I thank my fellow lab mates in the Paul Weiss group for the stimulating discussions and the willingness to provide assistance. I am grateful for the support from the National Science Foundation Integrative Graduate Education and Research Traineeship: Materials Creation Training Program (DGE-0654431), the Materials Science and Engineering Department at UCLA, the California NanoSystems Institute and the Kavli Foundation. Lastly, I would like to thank my parents for their continuous support in all my endeavors.

Chapter 1

Photoreactive Single-Molecule Systems

1.1 Introduction

Contemporary scientific research seeks to explore previously unobserved characteristics and interactions of novel systems in order to gain deeper understanding and control over the basic, physical concepts that order our world. Nanoscale science presents a unique opportunity to explore frontiers of scientific research that had previously remained theoretical. Understanding the electrical, magnetic, structural, optical, and mechanical characteristics at the nanoscale is essential to furthering the development of new techniques and devices. Synthetic control and developments in characterization methods of intermolecular interactions have led to advances in developing photoactive chemical species and the creation of novel optically active nanoparticles [1-3]. These photoreactive materials and phenomena yield great promise in energy and display applications [1-7].

1.1.1 Organic Photovoltaic Devices

Organic photovoltaic (OPV) devices promise inexpensive flexible replacements for traditional solid-state devices. The efficiencies of such organic devices have been reported as reaching as high as 15% [8, 9]; however, these efficiencies do not yet compete with traditional silicon-based solar cells, which easily provide efficiencies as high as 25% [10]. Organic solar cell power conversion efficiencies are collected from completed devices using:

$$n_{PCE} = \frac{V_{OC} \times I_{SC} \times FF}{P_{in}};$$

where FF represents the fill factor, defined as:

$$FF = \frac{I_{MP} \times V_{MP}}{I_{SC} \times V_{OC}}.$$

This efficiency is composed of four specified efficiencies specific to quasi-stable energetic states of the charge carriers:

$$n_{PCE} = n_A \times n_{ED} \times n_{CT} \times n_{CC} \ [11].$$

The absorption efficiency, denoted by n_A, corresponds to the photoactive region of the solar cell and the efficiency of exciton excitation. The charge transfer efficiency, n_{CT}, is the efficiency with which an exciton excited in a photoabsorber dissociates into free charge carriers at a donor-acceptor interface. The dissociation efficiency, n_{ED}, is the efficiency with which excited excitons can migrate to interfaces where they can be dissociated. The charge collection efficiency, n_{CC}, is the efficiency with which the charges, once split into free charges, are able to migrate to the electrodes. All of these terms innately depend on the characteristics of the molecules that compose the materials used in the device. Computational predictions aid in the initial selection of molecules to maximize device efficiency [12, 13]. Contemporary characterization techniques use incident photon-to-current efficiency measurement devices to ascertain the efficiencies of OPV devices. The currents and voltages, as seen in the power conversion efficiency and fill factor, which are applied or produced by the completed device are used to calculate overall power conversion efficiency [8-11, 14, 15]. The materials used to create these devices are characterized in bulk, determining absorption wavelengths via UV-Visible spectroscopy.

To increase the efficiency of the photoactive layer, the range of the solar spectrum that is absorbed by the photoactive layer must be widened, and the weak absorbance must also be

increased. Some approaches use low-band gap polymers that absorb into the infrared wavelengths of the spectrum, other approaches introduce metal nanoparticles [6, 16-18]. These nanoparticles exhibit local surface plasmon resonances (LSPRs), a property specific to metal nanostructures. Irradiation using wavelengths of light specific to the size and shape of the nanostructure induces a high electromagnetic field excited on the surface of the structures; this heightened field strength can increase the absorption of the devices organic materials. Metal nanoparticles incorporated into an organic medium increase the absorption efficiency of the organic material due to the heightened electromagnetic field generated by the LSPR. Periodic nanostructures introduced into the photoactive layer and the insertion of inorganic optical spacers between the metal electrode and the photoactive layer has increased light trapping [18-22]. Plasmonic enhancement using metal nanoparticles is also applied in molecular sensing, near-field optical microscopy, electrochromic devices, and light-emitting diodes [23-27].

1.1.2 Thesis Premise

This work focuses on utilizing photon-coupled scanning tunneling microscopy (photon STM) to investigate local surface plasmon resonances on triangular metal nanoprisms. The wavelength at which LSPR excitation occurs for individual nanoparticles is dependent upon the size, thickness, and shape, all of which can be controlled synthetically [26, 28-30]. The photon STM uses a total internal reflection scheme to couple light into the tunneling junction, generating this specific LSPR in individual Au and Ag nanoprisms. By controlling and coupling this specific excitation to molecular assemblies, the effective photoreactivities and photoconductances of organic molecules can be increased [18, 22]. Self-assembled monolayer (SAM) insertion strategies will be used to arrange single molecules and lines of molecules on Au{111} and Ag{111} nanoprisms for selective surface plasmonic enhancement. Photon STM

will also monitor the photoactivities of molecules on these substrates, such as photocurrent, photoconductance, and photoreaction, all essential characteristics for applications in OPV devices.

1.2 Self-Assembled Monolayers

The adsorption of alkanoic acid on a platinum surface was reported by Zisman *et al*. in 1946 [31]. This and earlier works defined monolayers created using such a process as SAMs. The structure and properties of the modified surface can be selected by changing the physical conditions during the deposition of SAMs onto a sample surface, or by changing the chemical properties of the species deposited [32, 33]. A multitude of surfaces can be functionalized by selecting molecule head groups that correspond to the desired substrate. RCOOH/Ni, ROH/Si, or $R(PO_4)_2$-/TiO_2 are all common headgroup/substrate combinations; however, the most frequently characterized systems are alkanethiols adsorbed on Au{111} substrates [34-36]. Alkanethiol SAMs are easily prepared and aggressively adsorb to the gold surface. The adsorption preference and stability observed in these systems are attributed to the strong gold sulfur bond (44 kcal/mol) and van der Waals interactions between alkyl chains (1 kcal/mol per methylene unit) [32]. Alterations to the tail group can affect the interactions between other molecules or particles [33]. Substituting the alkyl tail for photoreactive species enables the creation of various photoreactive assemblies, and the analysis of characteristics that define photoactive systems [37-40].

1.2.1 Defects

These alkanethiol SAMs, when imaged with STM, show characteristic features, including domains, domain boundaries, step edges substrate vacancy islands, and substrate adatoms

(Figure 1.1A). In order to maximize van der Waals interactions, each *n*-alkanethiol molecule is oriented with a tilt angle of 30° with respect to the gold surface normal (Figure 1.1B) [35, 39-41]. Depending on the tail length, the alkanethiolates form close-packed $(3 \times \sqrt{3})$ R30° lattices with respect to the underlying gold lattice for short (>11 carbon chain) molecules. Close-packed superlattices c(4x2) have been observed for longer chains. These phenomena have been attributed to stronger intermolecular interactions as compared to the sulfur-gold head group interactions [35, 42, 43]. Regions of ordered alkanethiol molecules that are aligned with the same tilt angles and lattice of attachment are considered a domain. In these homogeneous domains, the lattice spacing is observed to be 4.99 A [35]. The space between two converging domains with differing tilt directions or lattices of attachment is defined as a domain boundary [44-46]. The largest and most obvious features in a prepared sample are step edges. Step edges are boundaries between gold terraces that correspond to differences in height of one or more gold atoms. During deposition, alkanethiol molecules alter the surface energy of the gold atoms. During this period of heightened surface energy, gold atoms migrate across the surface, forming small lattices one atom lower than a gold terrace, substrate vacancy islands, or one atom above the terrace, substrate adatoms, with these atoms originating or ending at a different lattice [47].

1.2.2 Molecular Insertion

The defect sites described above are particularly important for the insertion of individual molecules into a host SAM. It is this method that enables the measurements of single-molecule conductivities, photoconductivity measurements, and photoreactions [48, 49]. It is through single-molecule measurements that we can ascertain the chemical characteristics of molecules used in solar devices and other functional materials. SAMs are formed by adsorbing *n*-alkanethiolate molecules to a sample surface using a solution of the desired alkanethiol diluted

into an appropriate solvent. For solution deposition, the sample is then submerged into the solution. For vapor deposition, the sample is sealed in a vial with a small amount of the alkanethiol solution at a temperature slightly below that of the solvent boiling point (Figure 1.2A). By allowing the SAM to form for longer periods of time, the host SAM is created with a higher degree of order, while conversely, shorter formation times lead to SAMs with lower degrees of order [44-48]. The target molecules were inserted either through solution deposition or vapor deposition at varying concentrations and varying times. Depending on the length and apparent height of these molecules of interest, the host alkanethiol height is chosen to be slightly shorter such that functional molecules to be measured protrude from the background SAM matrix. The specific molecules and concentrations will be discussed in later chapters. It was found that lower degrees of order in the SAM resulted in higher defect counts and larger defects [50-53]. The samples with high numbers of defects, acting as prime locations for molecular insertion, also have low degrees of order making sample stability sub-optimal for STM characterization. When imaged using STM, these inserted molecules appear as protrusions from the surrounding host SAM. (Figure 1.2B)

1.3 Scanning Tunneling Microscopy

Scanning tunneling microscopy measurements were first reported in 1981, and have taken a pivotal role in probing the electronic structure and molecular interactions on surfaces [54-56]. The theory and development of STM has since been explored in great detail [54-57]. Scanning tunneling microscopy is similar to other surface probe techniques in that a probe tip rasters across the surface collecting point data. When correlated, these images determine the topography in addition to other characteristics of a surface. An atomically sharp tip rasters across an electrically biased conducting, or semiconducting, surface. The data collected consists of the

minute fluctuations in current between the tip and the surface. The research described in this work utilizes ambient STM systems. Several STM schema require the collection of data in other media have been developed to investigate diverse systems [58-59]. Systems that couple simultaneous electrochemical measurements, electron microscopy measurements, alternate scanning probe microscopy measurements, and ultraviolet to infrared light excitation sources to STM have provided a wider range of information [60-64].

1.3.1 General Operation

Scanning tunneling microscopy uses low work function metals such as tungsten or a platinum-iridium alloy as an atomically sharp probe. As the tip is brought in close proximity to the sample, the electronic wavefunction of the tip overlaps with the electronic wavefunction of the surface. At such close distances electrons quantum mechanically tunnel from the tip to the surface through the potential barrier of the air separating tip and surface. The electron tunneling results in a small, but quantifiable, current between tip and sample, which changes depending on the position of the tip and the height and composition of the portion of the sample directly beneath it. The polarity of the bias applied across the junction determines if electrons tunnel from the tip to substrate or the substrate to the tip.

Tunneling is well understood through quantum mechanics. Electrons have a non-zero probability to tunnel through a potential energy barrier when the energy of the electron is less than that of the potential barrier. The waveform of the electron can be represented in a simplistic one-dimensional system in a rectangular potential barrier by the function:

$$\Psi(z) = \Psi(0)e^{-kz}.$$

With the wave number, *k*, corresponding to potential barrier of electron emission from tip to sample.

$$k = \frac{\sqrt{2m(V-E)}}{\hbar}$$

The wave function includes the specific conditions of each event, the tip height z, the mass of the electron m, V the potential energy of the barrier, and E the energy of the electron. From this wave function, we can also determine the probability distribution of the tunneling electron and from that, the tunneling current (Figure 1.3).

$$I(z) \sim |\Psi(z)|^2 \sim e^{-2kz}$$

In instances using small biases, it is appropriate to consider V-E to approximate the work function of the metal tip (~ 5 eV). It is then clear that the exponential current decay is approximately an order of magnitude per Ångström change in z [65, 66]. The correlation of current to minute changes in tip height enables atomically precise topographical imaging of surfaces. The tip-surface distance is generally manipulated in two modes of data collection: constant-current or constant-height mode (Figure 1.4). In constant-current mode, the most common scanning method, the tip rasters across the surface while the feedback loop maintains a constant, preset current by adjusting the distance between the tip and the sample. Constant-current mode provides higher precision due to its dependence on the geometric structure and the local density of states of both the sample and the tip. However, this higher precision comes at the price of slower scan rates due to the direct mechanical manipulation of the tip in the z direction. In constant-height mode, the tip is held at the same distance from the surface throughout scanning. This method scans faster, but at the cost of precision.

1.3.2 Photon-Coupled Scanning Tunneling Microscopy

Photon STM uses a total internal reflection to couple ultraviolet and visible light into the tunneling junction via backside illumination. Beams of light are directed through an optical layout where they are polarized perpendicular to the sample surface and modulated to match the lock-in amplification of the data collection. This is to induce illumination of the sample at those instances when data are being collected. Sample and illumination orientation are selected to maximize molecule excitation during data collection. The light is then focused onto the sample surface at a 54° angle via rear illumination (Figure 1.5), a microscope is used to ensure that the beam is focused to a point directly under the STM tip. The tip in this set up is manipulated using a microslider stage as opposed to the Besocke beetle, or piezoelectric walking, method [67,68].

1.4 Thesis Overview

This thesis primarily serves as an explanation of the methods developed to characterize single photoreactive or photoconductive molecules on a nanoprism platform using novel instrumentation. Chapter 2 will describe the synthesis and purification methods developed to synthesize gold nanoprisms. Chapter 3 will describe the process established to prepare suitable substrates to be used in photon STM and the procedure developed to deposit and to functionalize nanoprisms on the substrate surface. Initial results and conclusions will be presented in Chapter 3.

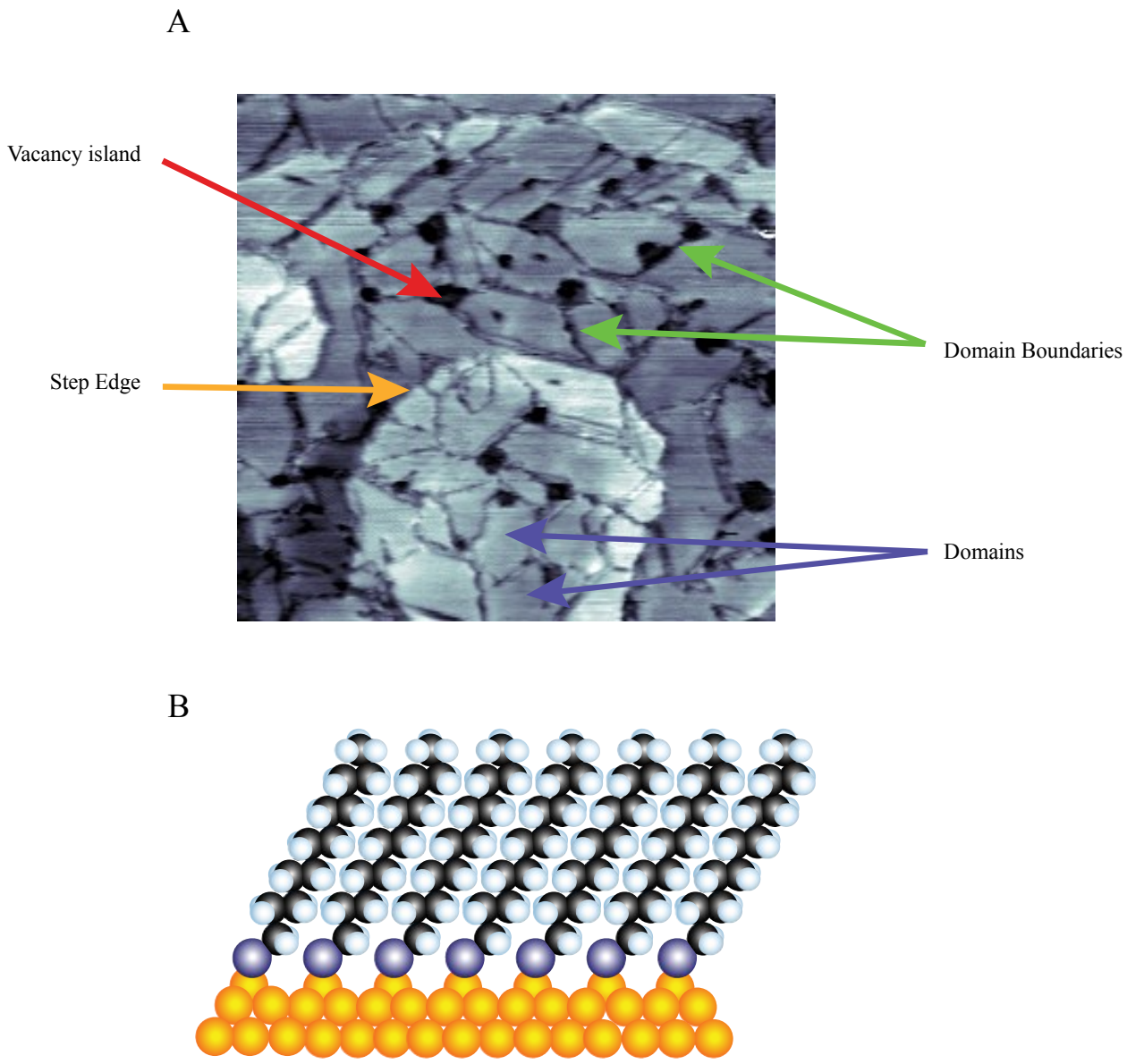

Figure 1.1: (**A**) Scanning tunneling microscopy image of dodecanethiolate SAM assembled on a Au{111} substrate. Characteristic defects within the monolayer are intrinsic to ordered SAMs and include vacancy islands (red arrow), step edges (orange arrow), domain boundaries (green arrow), and dodecanethiolate domains (violet arrow). Image is recorded with a sample bias, V_S = -1 V and tunneling current, I_T = 2 pA. (**B**) Schematic of a C12 monolayer, illustrating the packing and tilt of the molecules. Gold is represented by the gold circles, sulfur by the violet, carbon by the black, and hydrogen by the white.

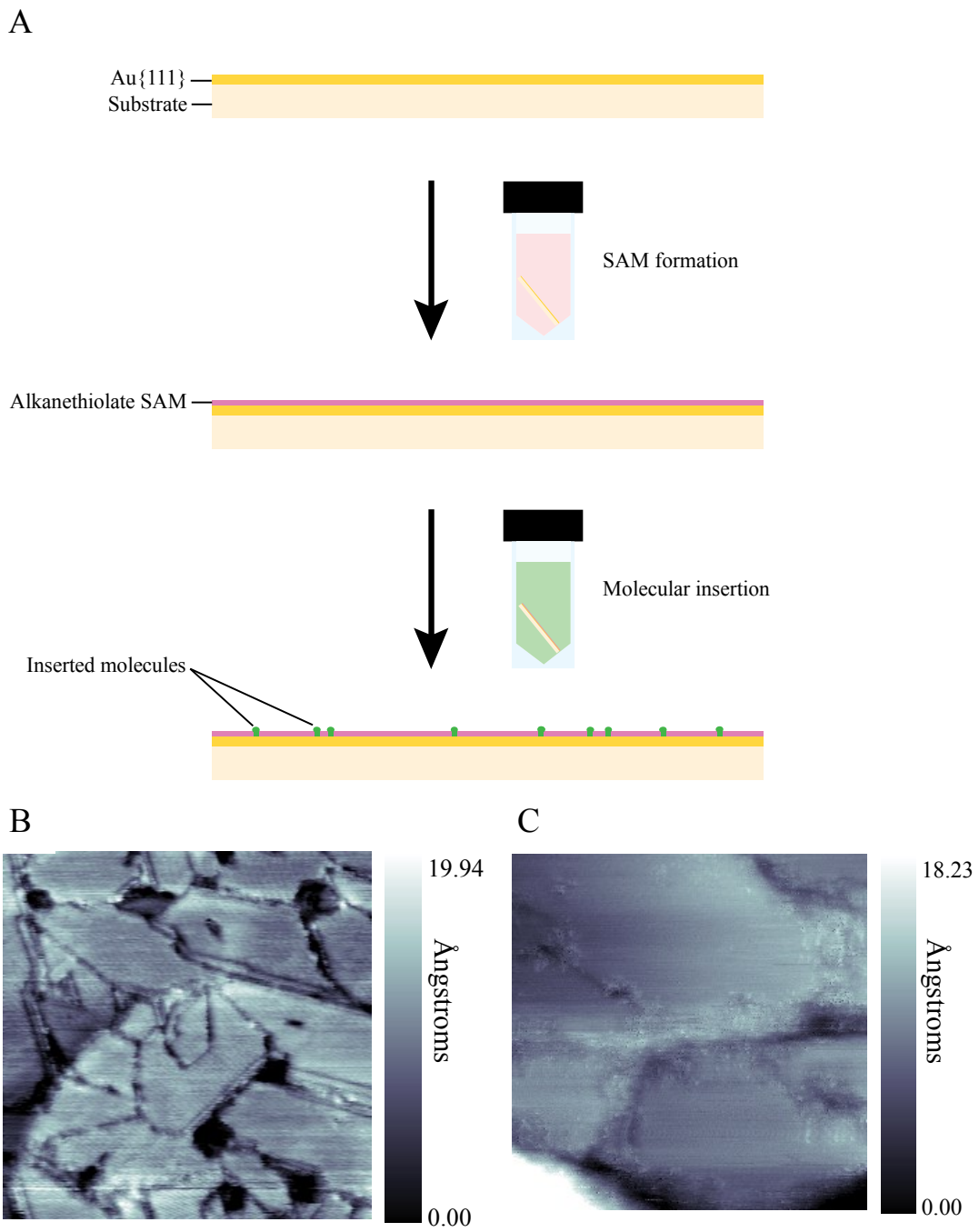

Figure 1.2: (**A**) Schematic of SAM solution assembly. Gold substrates are submerged in solutions of an alkanethiol dispersed in ethanol resulting in alkanethiol SAMs adsorbing to the sample surfaces. Samples functionalized with the alkanethiol SAMs are submerged in a solution containing the molecule to be inserted. (**B**) Scanning tunneling microscopy image of a 12-dodecanethiol SAM assembled on Au{111} substrate prior to insertion. (**C**) Scanning tunneling microscopy image of 9-(4-mercaptophenylethynyl)anthracene (MPEA) inserted into a 12-dodecanthiol background SAM. Images are recorded with a sample bias, V_S = 1 V and tunneling current, I_T = 1 pA.

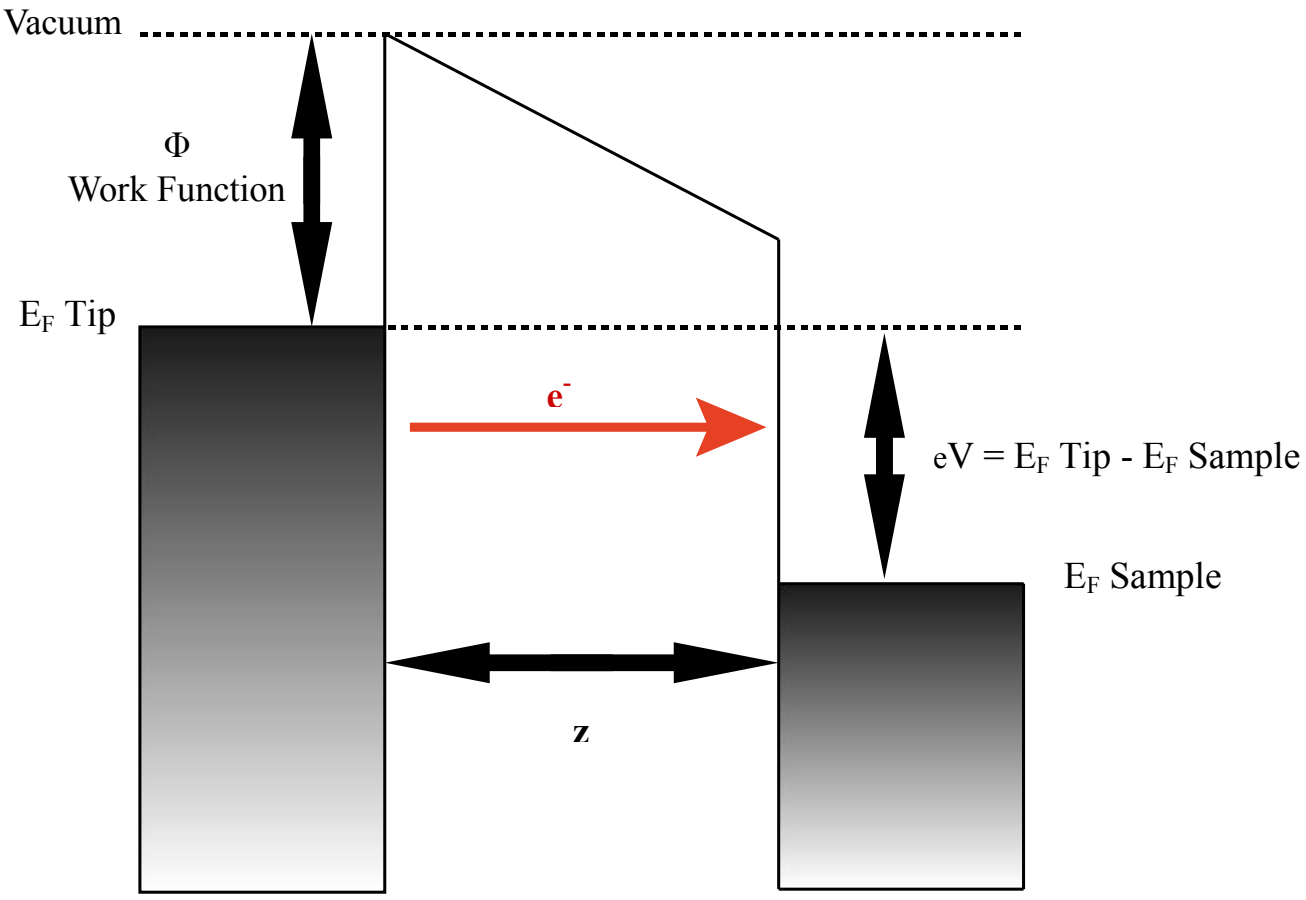

Figure 1.3: An energy level diagram for a one-dimensional electron tunneling junction. An applied bias voltage, V, offsets the Fermi energy, E_F, of the sample to the tip, which generates a tunneling current if the probe tip and sample are sufficiently close. The tunneling current is exponentially proportional to the distance between the tip and the sample surface, Z.

A

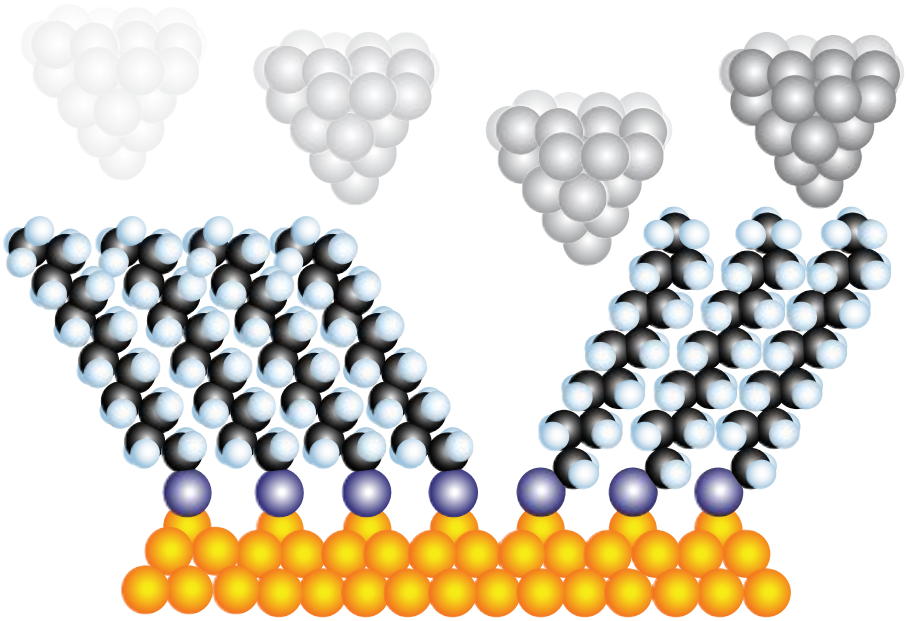

B

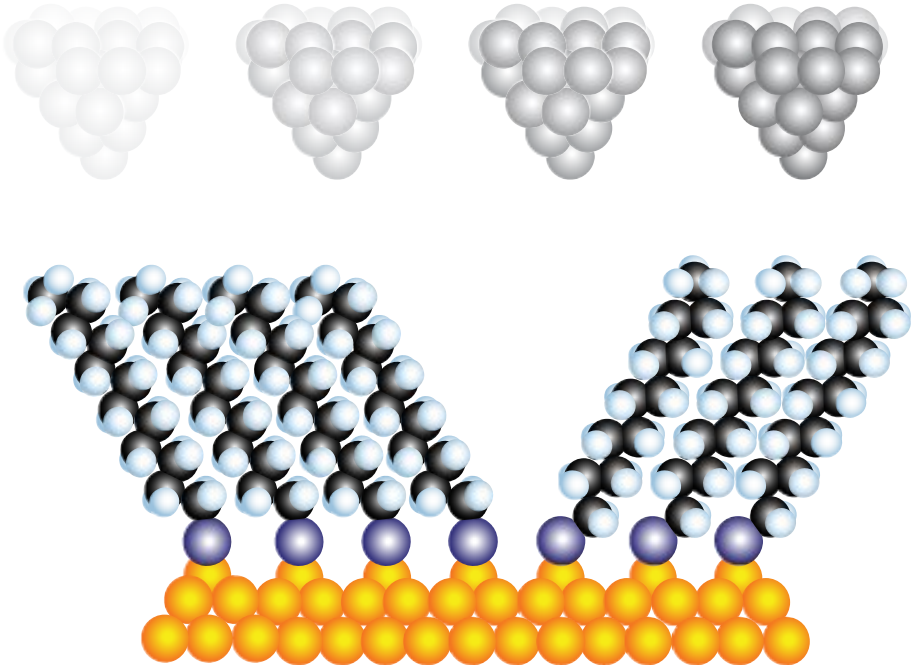

Figure 1.4: A schematic depicting the STM tip rastering across a 12-dodecanethiol SAM adsorbed to a gold surface. Data are collected in (**A**) constant-current mode, where the tip extension or retraction is collected while maintaining a constant tunneling current between the tip and sample, or in (**B**) constant-height mode, collecting the current fluctuations while the tip maintains a constant distance between the tip and sample.

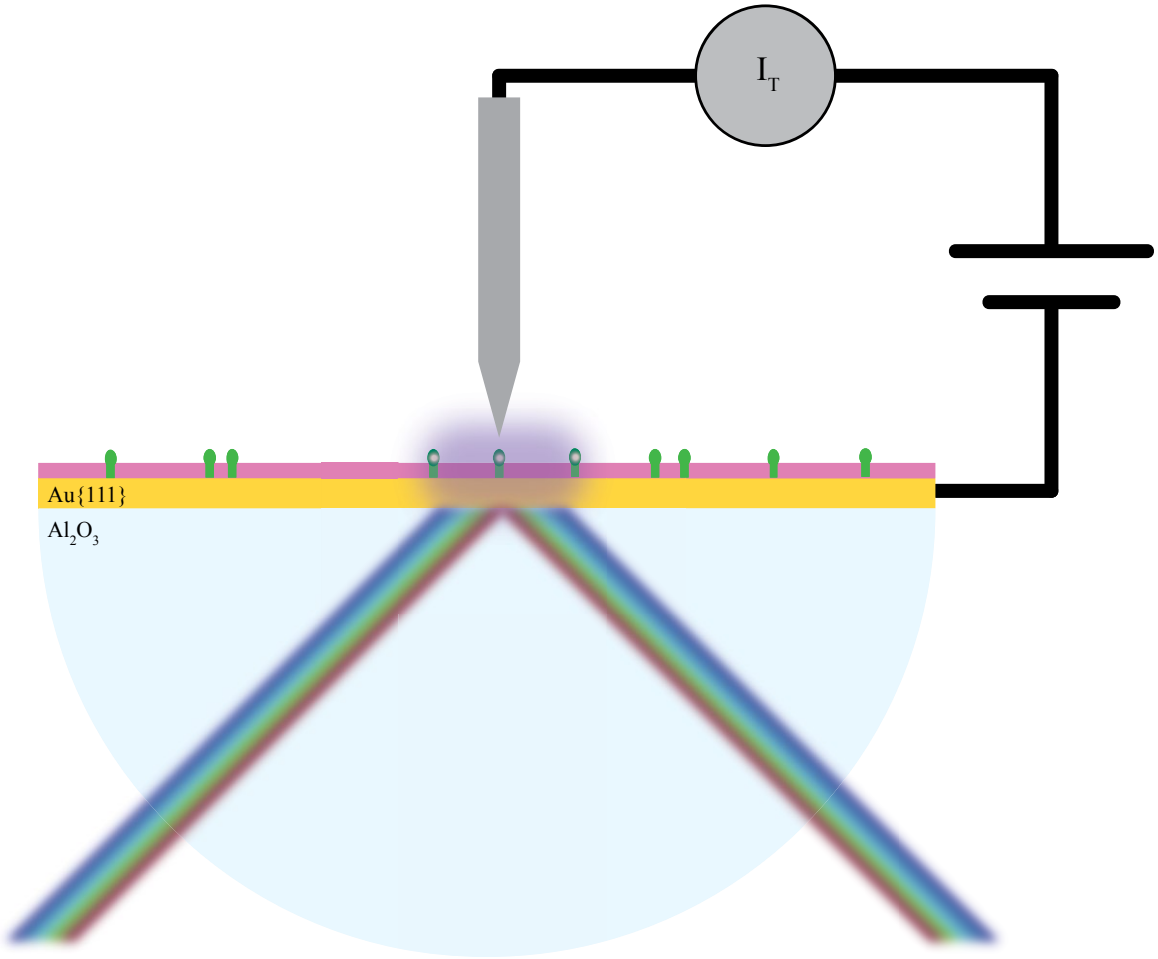

Figure 1.5: Schematic of the Photon STM tunneling junction. A thin gold film is evaporated onto a sapphire prism. A background alkanethiolate monolayer is adsorbed to the surface followed by molecular insertion of a photoreactive or photoconductive molecule. The tunneling junction is illuminated by the desired wavelength of light, while simultaneous topographic and electronic measurements are collected.

Chapter 2

Nanoparticle Synthesis and Preparation

2.1 Introduction

This chapter will discuss the synthesis and customization of nanoparticles to be applied in concert with the molecular systems discussed in chapter 1. The physical and optical properties of metal nanoparticles have been of great interest for centuries, some of the earliest work conducted on gold atom clusters by Michael Faraday in the mid 1800's [69]. Recent nanoparticle applications span many fields of research, including chemical sensing, spectroscopic enhancement, drug delivery, and nanostructure fabrication [70-73]. Growing applications of nanoparticles have necessitated precise control over the size, chemical composition, polydispersity, and geometry [74-77]. This work focuses on the development and application of nanoparticle geometries that provide atomically flat planes as platforms for single-molecule systems.

2.1.1 Isotropic Gold Nanoparticles

The gold nanoparticles utilized in this work are synthesized using a seed-mediated process as opposed to the photo-mediated process used for silver nanoprisms. These processes require isomorphous seed particles synthesized through the reduction of $HAuCl_4$ to gold clusters. Contemporary synthesis methods that follow this reduction route were developed from the efforts of Turkevitch et al. in the early 1950's [78, 79]. Colloid size has been controlled by altering the nucleation conditions, including gold concentration and the nucleation process. The smallest particles produced using this method measured approximately 150 nm in diameter, while subsequent work has produced particles with diameters under 15 nm [79, 80]:

$$6AuCl_4^- + C_6H_8O_7 + 5H_2O \rightarrow 6CO_2 + 24Cl^- + 6Au^0 + 18H^+.$$

This reduction of gold colloids using sodium citrate has led to current seed formation processes that favor sodium borohydride as the reducing agent [81-84]. The reduction of the gold ions is induced via the addition of a strong base; a weak reducing agent is then used to reduce additional gold ions onto the surface of the gold cluster resulting in growth of the nanoparticle of interest [83].

2.1.2 Anisotropic Gold Nanoparticle

Anisotropic nanoparticles inherently exhibit most of the basic characteristics of isotropic nanoparticles; however, the geometries of these particles offer unique photoelectric properties that expand potential applications including the development of nanoparticle assemblies and surface enhanced Raman spectroscopy (SERS) [85-88]. In this work, the surface-enhanced optical and electronic properties, in addition to physical topography, of anisotropic nanoprisms are integral to the creation of nanoprism single-molecule systems. Variations in particle geometry and size alter specific extinction spectra and electromagnetic fields [28], which will be explained in Chapter 3. Control over nanoparticle geometry has significantly increased in the past ten years, allowing the synthesis of a plethora of anisotropic shapes including rods, bipyramids, icosahedra, among other complex structures using several processes [89-93]. Integral to particle stability in solution is the formation of a protective micelle, either through ligand attachment or surface charge, to prevent aggregation [94-96]. The rate of ion reduction onto particular planes of the nanoparticle dictates the final shape of the nanoparticle. These conditions are controlled by precise selection and control of the synthesis conditions, which alter the plane selectivity of ion reduction [83]. Photo-mediation and seed-mediation are two of

several mechanisms that govern particle formation, and are the mechanisms that are central to this work. Each limits the final nanoparticle size by restricting ion reduction onto initial isotropic seed particles. By precisely controlling the photonic excitation of the particles, temperature of synthesis, concentrations of constituent materials, and ligand binding properties; different shapes, sizes and homogeneities of produced particles can be synthesized [29,81, 97].

2.2 Experimental Section

2.2.1 Materials

Tetraurochlorate, hexadecyltrimethylammoniumbromide (CTAB), sodium borohydride, potassium iodide, and ascorbic acid were all purchase from Sigma-Aldrich. L-ascorbic acid was purchased from Fisher Aldrich. All water used in this work was purified using a Millipak Express, where particulate matter was removed via a 0.22 μm filter. All glassware was cleaned using aqua regia and generously rinsed before use.

2.2.2 Gold Nanoparticle Synthesis

Synthesis methods developed in this study originated in previous works synthesizing the desired nanoparticle geometries [82-84]; however, differences in results necessitated significant alterations to the procedure. All syntheses originate with a seed solution synthesized using the procedure developed by Chad Mirkin *et al*, at Northwestern University [81]. Deviations in results necessitated additional environmental controls to reproduce the desired nanoparticle geometry and monodispersity. The initial gold seed solution, which provides nucleation sites for particle growth, consists of ~5 nm faceted, isotropic nanoparticles, reduced from aqueous gold salt using sodium citrate. An aliquot of this solution was then used to initiate a multi-step growth process in an aqueous gold salt solution. Once the seeds are added to a gold ion growth solution,

selecting conditions that determine selective plane adsorption is essential in controlling the final particle geometry. The presence of iodide ions, either through the addition of potassium iodide or as an impurity in the CTAB, determines edge selectivity of ion adsorption [83, 84]. Temperature of the growth step will also determine final particle geometry [83]. Through the selection of these two conditions, isotropic polygonal nanoparticles, nanorods, and nanoprisms have all been synthesized. Controlling additional environmental conditions such as gold concentration, solution pH, and gold seed concentration allow for selection of particle size and concentration [98].

2.2.1.1 Gold Seed Particle Synthesis

The seed solution detailed herein is a common method of synthesizing isotropic gold particles approximately 5 nm in diameter [82-84, 99, 100]. One milliliter of a 100 mM sodium citrate solution and 1 mL of 18 mM tetraurochlorate were added to 36 mL of stirring 18 MΩ water. One milliliter of freshly prepared 50 mM sodium borohydride was then added to the solution inducing a color change of light yellow to burgundy. Previous methods have used chilled sodium borohydride solutions; however, no temperature correlations were observed. The solution was then stirred for one minute, after which, the solution sat undisturbed for one hour to allow full reaction of the sodium borohydride. The seed solution was then analyzed using ultraviolet-visible spectroscopy (Figure 2.1) with a resulting absorption peak at 531 nm. Seed solutions were kept in an ambient environment at room temperature for up to four weeks without any discernible quality deterioration. Electron microscopy images of the seed solution are displayed in Figure 2.1b.

2.2.1.2 Gold Isotropic Nanoparticle Synthesis

Two methods were developed during this work to synthesize anisotropic gold nanoparticles. Each method initially followed an established procedure, which required several alterations to synthesize monodisperse nanoprisms consistently given different environmental conditions. One method used a multi-step growth process; the other used a single-step growth process [71, 83]. The multi-step procedure uses three growth solutions containing gold ions in a ligand saturated solution. A 9 mL solution of 0.1 M CTAB was prepared by dissolving solid CTAB into 35 °C deionized water. Once completely dissolved, the solution was removed from heat and 0.25 mL of 10 mM $HAuCl_4$ was then added, inducing a change in color from colorless to dark yellow. With the addition of 0.5 mL of 400 mM ascorbic acid the solution became colorless, indicating the reduction of the gold salt to gold ions. This process was repeated to prepare a second solution, and a third growth solution was prepared by scaling up the volumes used for the previous two solutions by a factor of ten. This third growth solution was prepared in a 250 mL round bottom flask. During the preparation process the solutions were allowed to cool to room temperature. One milliliter of the gold nanoseed solution was added to the first growth solution and mixed using a pipette. After 2-4 seconds 1 mL of the first solution was added to the second growth solution and again mixed using a pipette. After another 2-4 seconds, all of this second growth solution was then added to the third, large growth solution at which point the solution was gently shaken. The solution gradually shifts from colorless to violet over the next five minutes. This solution was then allowed to sit at room temperature for a minimum of three hours.

The single step process follows a similar method of using seed particles as nucleation sites in an ion rich growth solution. A 97.5 mL 50 mM CTAB solution was prepared in a 250 mL

beaker. The solution was prepared using 35 °C deionized water to allow for complete CTAB dissolution. The addition of 2.5 mL of a 10 mM $HAuCl_4$ solution induced a color change of the growth solution from colorless to dark yellow. A subsequent addition of 550 uL of 100 mM ascorbic acid returned the solution to colorless. A 550 uL addition of 100 mM sodium hydroxide was added to neutralize any remaining ascorbic acid and provide a final pH of 4. The solution was then moved to an incubator maintaining a temperature of 27 °C. One hundred microliters of gold nanoseed solution was added and a color change from colorless to violet was observed over five minutes. The solution was then allowed to sit overnight at 27 °C to allow for complete nanoparticle formation.

Following these synthesis procedures, two methods of producing isomorphous heterogeneous polyhedral nanoparticles were developed. These nanoparticle solutions consisted of cubes, short rods, polyhedral shapes, nanoprisms, truncated platelets, and small residual isotropic particles.

2.2.1.3 Gold Nanorod Synthesis

Delineating nanoparticle growth from isotropic to anisotropic requires the encouragement or inhibition of selective side growth. Altering the single-step synthesis by lowering the temperature of the growth solutions, and allowing the nanoparticle growth to proceed in a water bath at 15 °C induces the formation of nanorods. A byproduct of 20 nm isomorphous polyhedral nanoparticles is present in the final solution. The multi-step procedure results in large volumes of nanorods, once separated from the bulk isomorphous solution. In both methods, increasing the gold concentration results in nanorods with higher aspect ratios, while adding larger volumes of nanoseed solution produces nanorods with smaller aspect ratios.

2.2.1.4 Gold Nanoprism Synthesis

Nanoprism growth was initiated in both methods with the introduction of a ligand inhibitive ion, in this work, sodium iodide. An addition of 1 mL of 1.86 mM sodium iodide was made to the multi-step procedure. In the single-step process 10 uL of 100 mM sodium iodide was added. By increasing or decreasing the iodide concentration the nanoprism sharpness can be altered, allowing for a high population of hexagonal and severely truncated plate structures in the case of higher iodide presence, and rice like structure in the case of lower iodide concentrations. Nanoprism size reacts similarly to nanorod synthesis with alterations in gold concentration and seed addition.

2.2.3 Silver Nanoprisms

The synthesis process of silver nanoprisms also relies on the selective adhesion of silver ions to seed particles in a process similar to that of gold nanoprisms. However, instead of relying on the previously described thermal syntheses, the innate optical properties of the metal nanocrystals are excited. The photochemical reaction initiating growth involves charge transfer of adsorbates and "hot" holes produced by plasmon recombination [97]. These positively charged silver ions produced in the dissolution of small silver particles are reduced onto the surface by the trisodium citrate ligand stabilizing the particle.

$$2Ag^0 + ½\ O_2 + H_2O \rightarrow 2Ag^+ + 2OH^-$$

As the particles are illuminated with specific wavelengths of light correlating to the dipole SPR of the nanoparticle, the excitation of energy is localized in the tips of particle. The face selective silver reduction is an effect of this localized excitation.

2.2.3.1 Silver Seed Particle Synthesis

In a 250 mL three neck round bottom flask, 95 mL of deionized water was cooled to 0 °C in an ice bath, at which point, argon was bubbled through the water. During this purging step, the flask was isolated from light and sealed to prevent excess exposure to oxygen. After 30 minutes 1.0 mL of 30mM sodium citrate and 0.5 mL of 20 mM $AgNO_3$ were added. After which, 1 mL of freshly prepared, ice cold 50 mM $NaBH_4$ was added. Every 2 minutes over the following 14 minutes, 5-6 drops of 50 mM $NaBH_4$ was added. A solution consisting of 1 mL of 50 mM $NaBH_4$ and 1 mL of 5 mM BSPP was added drop wise over 3 minutes. Following this addition, the solution remained colorless. Argon was bubbled through the stirred solution while submerged in an ice bath for a minimum of 5 hours in complete light isolation. The solution was then allowed to age, undisturbed, overnight while still isolated from light at 4 °C. Following this aging process, the solution was found to be a light yellow.

2.2.3.2 Silver Nanoprism Synthesis

The solution was then exposed to two (Phillips F28T5 Silhouette) lamps for a minimum of 48 hours. Longer exposure results in a higher yield of complete nanoprisms, with a corresponding decrease in truncated nanoprisms and residual nanoplates.

2.2.4 Nanoparticle Purification

The synthesis processes detailed in this chapter, like many other methods, do not produce homogeneous particle distributions. The majority of particles formed are those of interest; however, it is common to find substantial residual particles or particles that have not completely formed. Segregating these particles in order to retain only those of the desired dimensions can severely complicate the overall synthesis process. The multi-step approach used for gold

nanoparticles proves much more difficult to purify. This approach also has an excessive amount of CTAB in solution, which when cooled to room temperature crystallizes and complicated subsequent nanoparticle analysis and deposition. To separate these products, solutions prepared using the multi-step process were filtered using Whatman Anodisc 25, 100 nm pore size filters, then briefly sonicated and dispersed in 18 MΩ deionized water. These solutions were then centrifuged and dispersed in 18 MΩ deionized water to further remove any excess CTAB remaining in solution.

The single-step process produces a solution of much lower CTAB concentration, such that when the temperature cools to 25 °C a transparent purple color remains with no signs of precipitation. Nanorods and nanoprisms were isolated by allowing the solution to rest undisturbed overnight in an incubator set to 25 °C. The remaining growth solution was poured out being careful to leave the nanorod or nanoprism precipitate undisturbed. This precipitate was then dispersed in 5 mL of 10 mM CTAB. Brief sonication was applied to completely disperse the precipitated nanorods or nanoprisms.

2.3 Results and Discussion

2.3.1 Gold Isotropic Nanoparticles

Scanning electron microscopy was used to verify the quality of synthesis procedures and determined the key conditions which resulted in alternate shape formation. The isotropic nanoparticle synthesis processes, results in solutions containing a heterogeneous mixture of isotropic polygonal, rod shaped, and prism shaped nanoparticles as seen in Figure 2.2. It is evident from the composition, small size of the particles (approximately 50 nm in diameter), and

small percentage of nanoprisms that anisotropic growth has been stunted although not completely prevented.

2.3.2 Gold Nanorods

Decreasing the temperature at which the multi-step process growth occurs induces a drastic change of nanoparticle morphology. A heterogeneous mixture (Figure 2.2) of nanorods, with lengths over 200 nm, and nanoprisms, with diameters of approximately 160 nm, resulted from this synthesis. Purification of single-step solutions produced homogenous nanorod solutions (Figure 2.3).

2.3.2 Gold Nanoprisms

The final alterations to the multi-step process, which included the addition of potassium iodide to the growth solution, resulted in a homogeneous solution of nanoparticles. It has been suggested that the iodide ions form an adlayer on the nanoparticles during growth. A CTAB layer that is more stable than that formed in the base procedure forms on this adlayer and regulates the adhesion of gold salt ions to the particle. The vertices of the prisms provide surfaces with weaker bonding of the protective ligand bilayer, which encourages higher rates of nucleation [83]. This high growth rate on the edges causes the plate-like structure of the nanoparticles, while the initial polygonal geometry of the seed particles ensures the prism-like shape. Upon post analysis the average size of the nanoparticles was found to be 0.0105 μm^2 with a standard deviation of 0.003 μm^2. Manual analysis of prisms diameters, from tip to mid base, revealed an average diameter of 140 nm. Line scans of atomic force microscopy (AFM) images determined the average thickness of the nanoprisms was determined to be 9 nm (Figure 2.5). Images were taken at high resolution to verify the surface structure of the gold nanoprisms. High

resolution transmission electron microscopy (TEM) images resolved the atomic structure of the nanoparticle surfaces to be that of Au{111} (Figure 2.6).

2.4 Conclusion

Strict control of the growth conditions is necessary to synthesize homogeneous, anisotropic nanoparticles. Using both the single step and multi-step methods we were able to synthesize and to purify homogenous solutions of gold isotropic particles, nanorods, and nanoprisms. Altering the reactant concentrations allowed control of the dimensions of the final nanoparticles. Silver nanoprisms were also synthesized; however, further work on the application of silver nanoprisms as substrates has yet to begin.

A

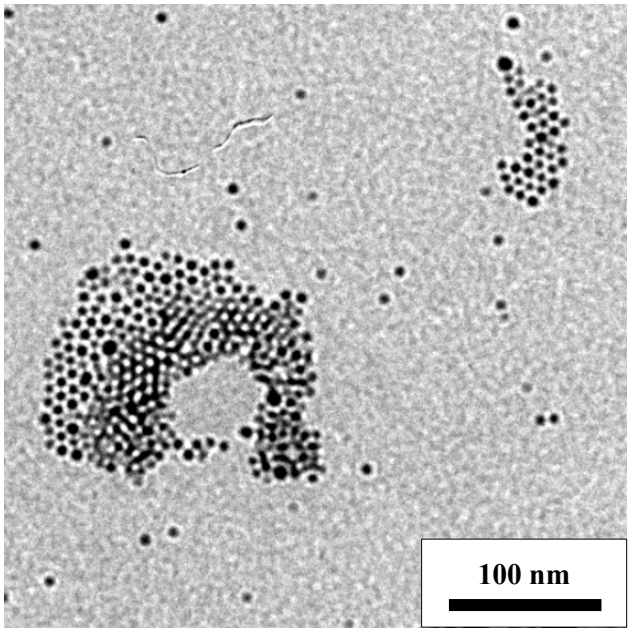

B

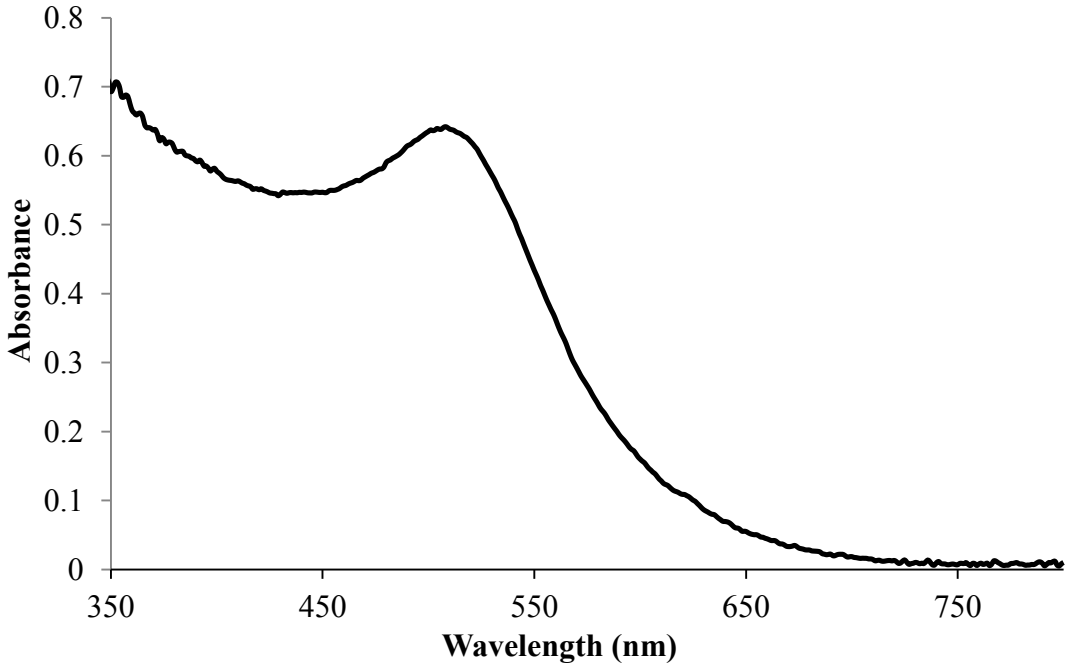

Figure 2.1: (**A**) Transmission electron microscopy image of citrate stabilized gold nanoseeds. (**B**) An absorption spectra of gold nanoseed solution.

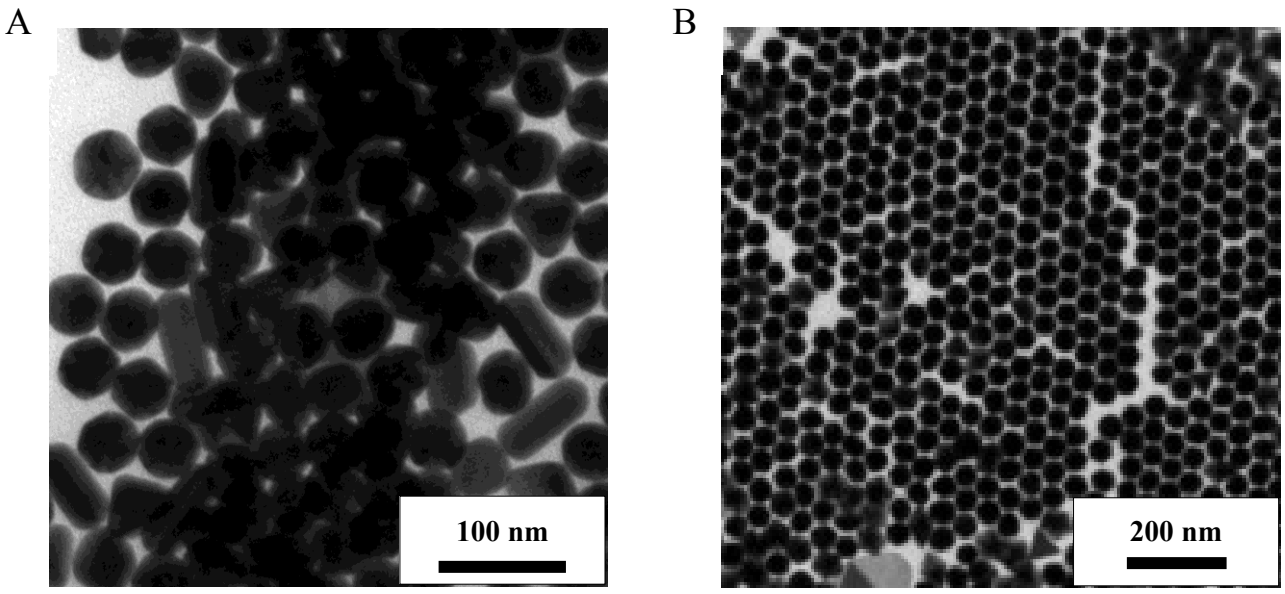

Figure 2.2: Transmission electron microscopy image of isotropic gold nanoparticles synthesized using the (**A**) multi-step process and the (**B**) single step process.

A

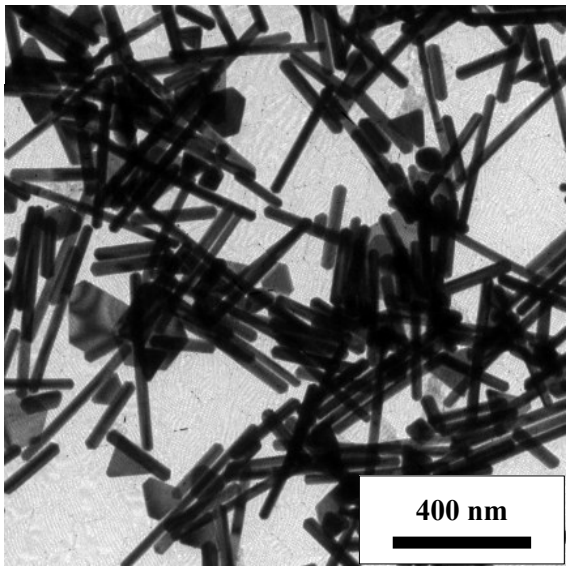

B

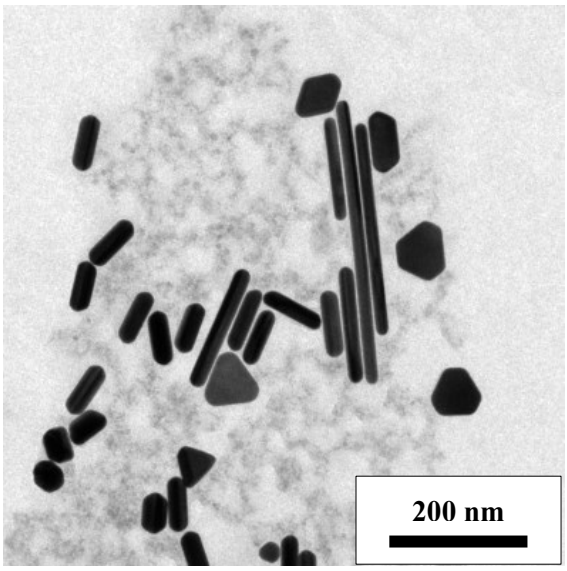

Figure 2.3: Transmission electron microscopy image of gold nanorods synthesized using the (**A**) multi-step process and the (**B**) single step process.

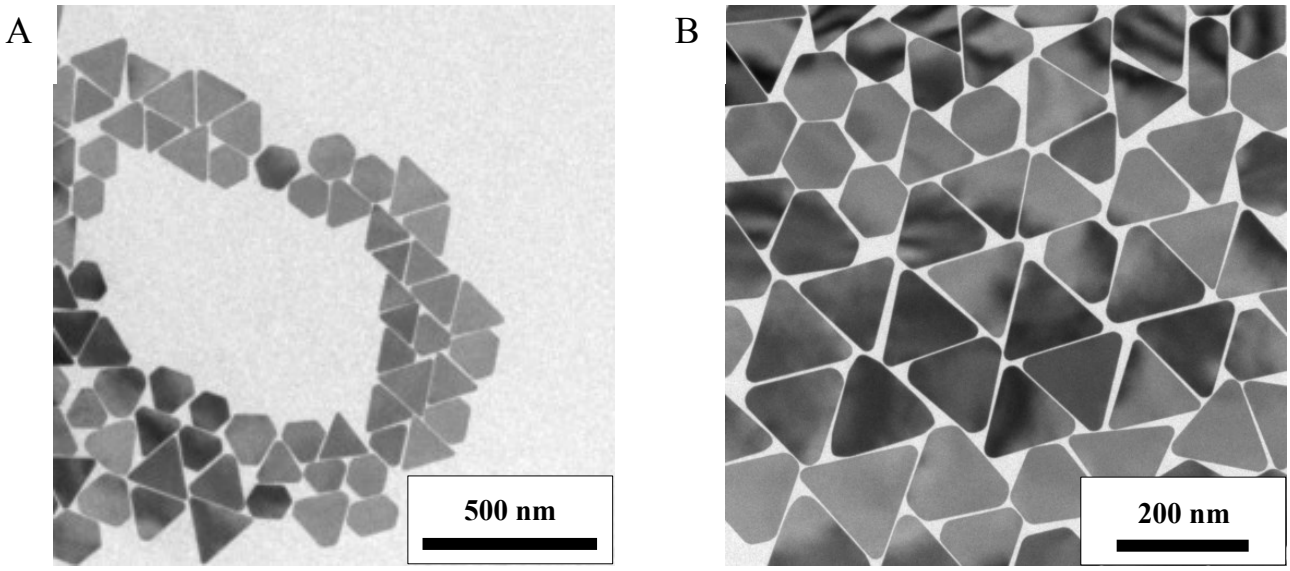

Figure 2.4: Transmission electron microscopy image of gold nanoprisms synthesized using the (**A**) multi-step process and the (**B**) single step process.

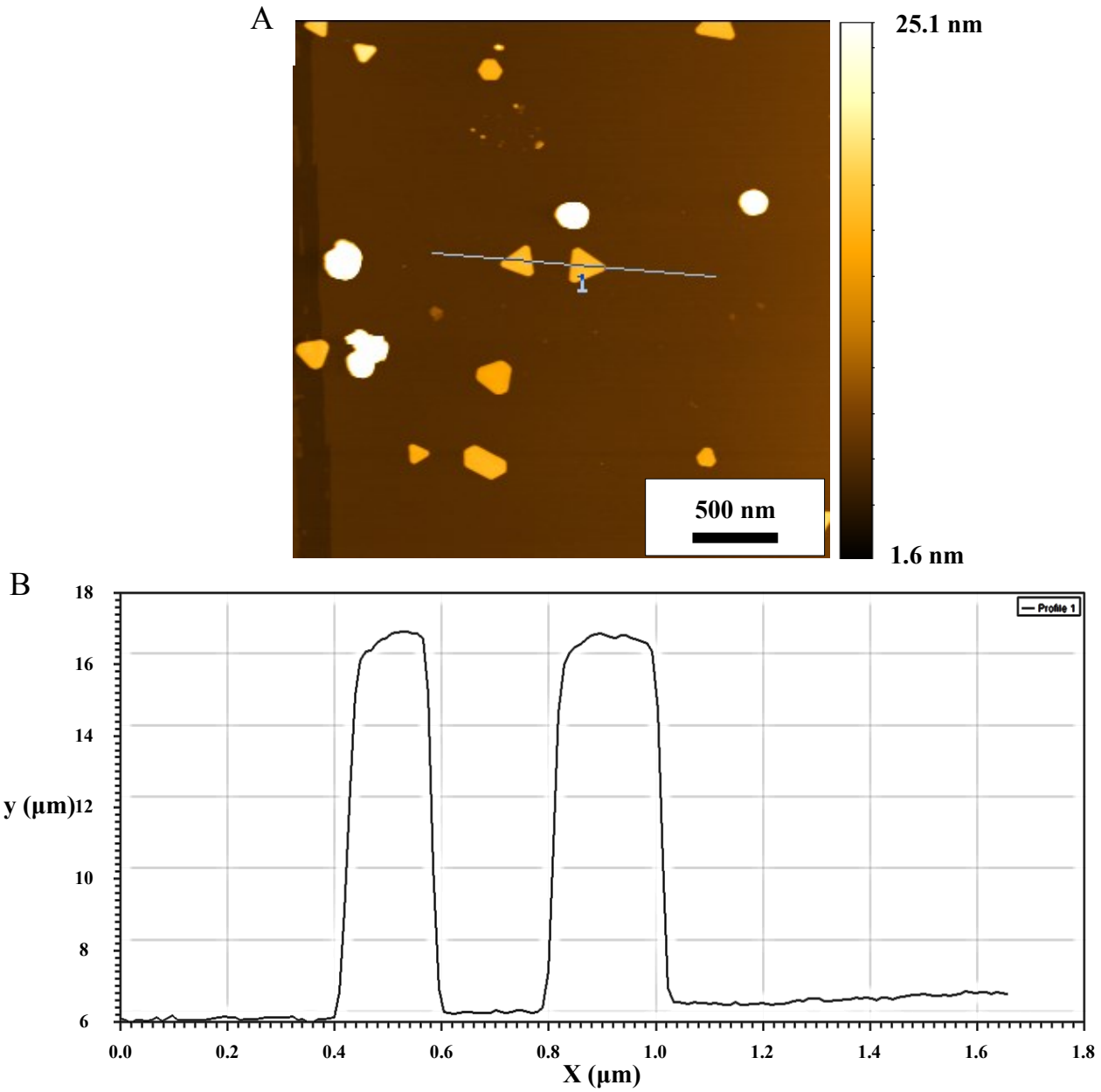

Figure 2.5: (**A**) Atomic force microscopy image of gold nanoprisms deposited on mica. The line corresponds to (**B**) a topographic profile extracted from the recorded image.

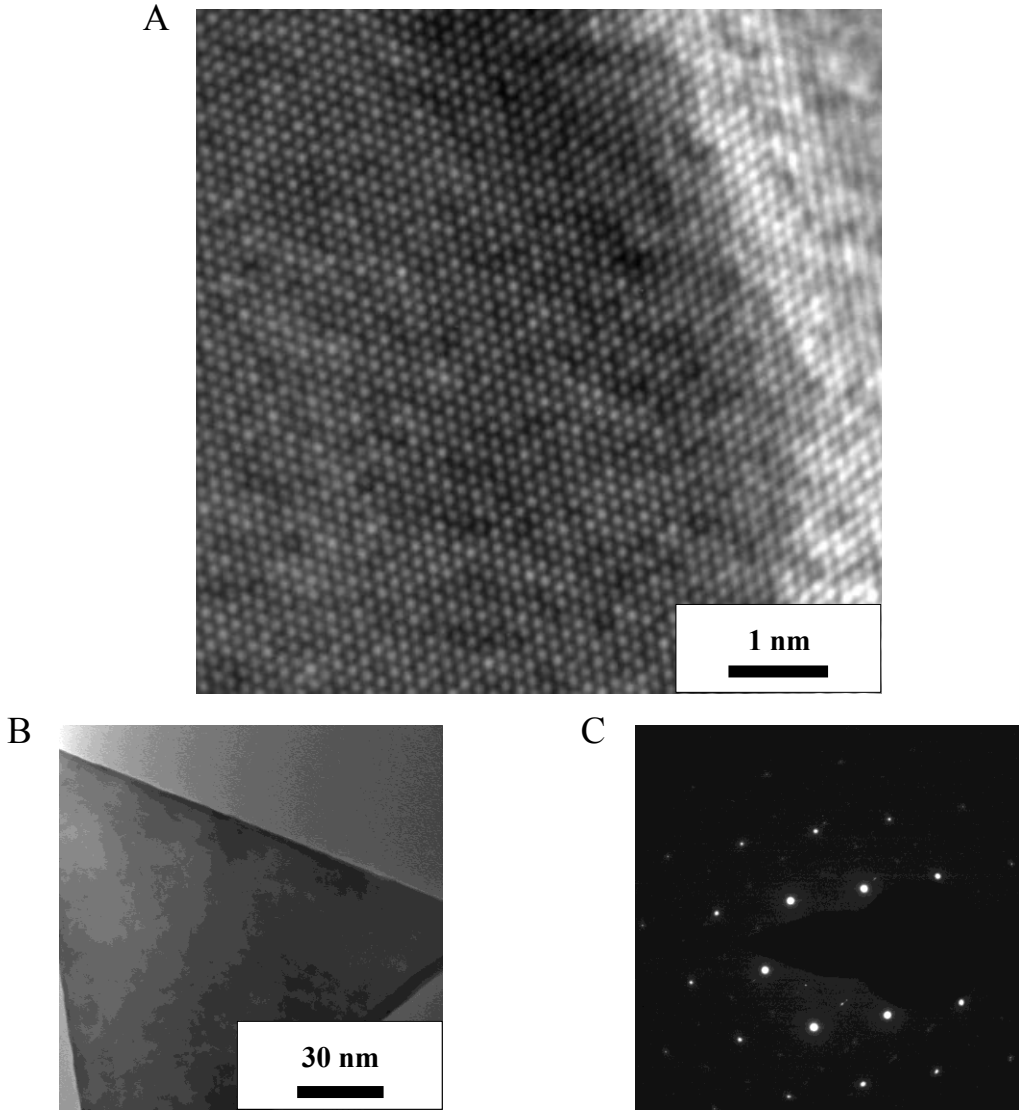

Figure 2.6: (**A**) High-resolution TEM image of the atomic structure of the corner of (**B**) a single gold nanoprism. (**C**) Diffraction pattern of a gold nanoprism.

Chapter 3

Nanoparticle Synthesis and Preparation

3.1 Introduction

Photonic coupling of nanoparticles and organic materials offers promising enhancements in a variety of OPV devices [101,102]. However, the characterization of precise interactions that govern these applications have focused on bulk phenomena [100-103]. Analysis of the coupling interactions between individual particles and surrounding molecular systems will provide a deeper understanding of precise photonic responses that are averaged in bulk measurements [103-108].

3.1.1 Local Surface Plasmon Resonance

Noble metal nanoparticles have been of great interest since the early 1800's. A notable result of such exploration is the application of gold nanoparticles to create vibrant red coloring in stained glass [109]. These particles exhibit a response to specific wavelengths of light called LSPR. Surface plasmon resonance (SPR) was first observed in the unexpected diffraction produced by diffraction gratings by Wood in 1902; a result of the excitation of surface plasmon waves in the grating [110]. In the late 1960's Kretschmann and Otto were able to excite surface plasmons on smooth surfaces, using the evanescent wave present in total reflection [111,112]. The plasmonic phenomena first exhibited in these works have been studied extensively and the observed properties have been presented in many works [110,113]. Surface plasmon resonance is a charge-density oscillation that exists at the interface of two materials with opposing dielectric constants, i.e., a metal and a dielectric [110]. The surface plasmon wave (SPW) is generated via electromagnetic excitation. This excitation is maximized at the interface, and decays

evanescently into both materials. The generated SPW is perpendicular to the direction of travel and is parallel to the plane of the interface. The propagation constant of the SPW propagating along the interface can be described using the expression:

$$\beta = k\sqrt{\frac{\varepsilon_m n_s^2}{\varepsilon_m + n_s^2}}.$$

Where k is the free space wave number, $\varepsilon_m$is the dielectric constant of the metal, and $n_s$is the refractive index of the dielectric [110]. A simple analysis of this expression demands that a propagating SPW obeys the relationship: $\varepsilon_m < -n_s^2$. Several metals exhibit this dielectric constant at optical wavelengths; however, gold and silver are favored due to robust existing synthesis methods [110]. Surface plasmon waves propagate along the interface of metal and dielectric materials over distances on the order of tens to hundreds of microns. The waves decay evanescently in the z-direction at a rate proportional to the inverse of the electron decay length; on the order of 200 nm [114-116]. Metal nanoparticles are consistently smaller than the propagation lengths of SPWs and the wavelength of incident light. This resulting plasmon oscillates locally around the nanoparticle. (Figure 3.1) The frequency at which this oscillation occurs is the LSPR [28,117,118].

An explanation of LSPR was first presented in 1908 by Mie, where a solution to Maxwell's equations described the extinction spectra of nanoparticles [119-122]. The Mie solution has proved accurate for spherical particles of arbitrary size; however, additional interests in novel applications require an extension of this theoretical explanation to particles with unique geometries, sizes, and material compositions [28,122,123]. Several techniques are now used to describe the LSPR response exhibited by a plethora of particles and environments of recent

interest [28]. Metal nanoparticles, when irradiated, are subject to the oscillating electromagnetic field inherent to the irradiating light. This electric field causes a complementary, coherent oscillation of conduction electrons. The electron cloud, when displaced from the nanoparticle by the electric field, is subject to a columbic restoring force between the electrons and nuclei. This restoring force is the cause of oscillation of the electron field with respect to the nuclear position of the nanoparticles. The frequency of oscillation is determined by the size, shape, the density of electrons, and the effective mass of the electrons in the particle [28,124]. These factors also determine the order of plasmon excitation. The coherent resonance of the entire electron field is called the dipole plasmon resonance. The oscillation of one half of the electron cloud parallel to the electric field and the other oscillating anti-parallel is termed quadrupole plasmon resonance [28]. Further plasmonic resonance modes have been observed and theorized; however, most nanoparticle geometries are dominated by dipole and quadrupole resonances.

3.1.2 Environmental Variables of LSPR

The electron cloud oscillation frequency is determined by the four factors listed above. However, the resonance frequency of the LSPR is dependent on the size, shape, dielectric properties, and the local environment of the particle [48,125-129]. Several approaches describe the effect of particle size and shape on LSPR frequency, most of which expanded on the Mie solution to describe particles of arbitrary shape and size [28]. The local surface plasmon resonance of a system is sensitive to the dielectric properties of the medium and particularly the refractive index of the dielectric in close proximity to the metal-dielectric interface [130-135]. The presence of a solvent surrounding the particle, a stabilizing ligand, an underlying substrate, and even coupling interactions between neighboring particles all influence the LSPR of a nanoparticle [136-139]. The resonant wavelength of gold nanoparticles red shift as the refractive

index of the suspending solvent increases. Polar solvents display charge-transfer interactions with the gold surfaces, which exhibit a high electron affinity [140]. Depending on the surrounding solvent, gold particle surfaces withdraw or donate an electron, which enhances the LSPR shift [124]. It has been reported that increasing the solvent chain length will produce a blue shift in observed LSPR wavelength. Longer chains prevent diffusion to the particle surface, preventing electron donation to the gold particles. Accordingly, shorter chains enable diffusion to the particle surface, allowing higher rates of electron donation to the gold particle. This produces a red shift excitation wavelength of the particle LSPR [124]. Stabilizing the nanoparticles is necessary to preventing particle degradation and aggregation. To this effect, the introduction of stabilizing ligands is necessary during nanoparticle growth syntheses. The ligand shell surrounding a nanoparticle is analogous to encapsulating the particle with a medium that exhibits different dielectric properties, and thus a refractive index that differs from the metallic core. Increasing the refractive index of the dielectric immediately surrounding a nanoparticle alters the previously homogeneous interaction of the electromagnetic field on the particle. This change can be approximated to altering the dielectric constant of the particle causing a red shift of the excitation wavelength of the LSPR [124]. Increasing or decreasing the thickness of the ligand shell will shift the LSPR wavelength accordingly [130,131,133-135,141,142]. The functionalization of particle surfaces with select ligands results in LSPR shifts, dampening, or enhancement depending on the molecule used [143].

The supporting substrate composition is a critical factor in determining the LSPR peak wavelength of deposited nanoparticles. The dielectric properties of the substrate, shape deformation or wetting by the substrate, and charge transfer at the particle/substrate interface are all critical interactions, which can cause LSPR wavelength shifts [143,144]. The systems used in

this work consist of gold nanoparticles on gold substrates. Dielectric characteristics of gold nanoparticles should closely resemble that of bulk gold. Thus, the role of charge transfer at the particle-substrate interface should be minimized [145]. It has also been observed that the sensitivity factor, $\Delta\lambda_{max}/\Delta n_{substrate}$, or LSPR dependence on substrate refractive index is 87 nm per refractive index unit (RIU) experimentally and 155 nm per RIU using discrete dipole approximation (DDA) [145].

In addition to the environment that has been selected to characterize individual nanoparticles, the interactions between nearby nanoparticles generally overpower the single-particle properties [138]. Two nanoparticles in close proximity will induce plasmonic electric field interactions [146-150]. The electric field experienced by each particle is a combination of the field induced by incident light and the electric field of the neighboring particle [146]. The interaction between nanoparticles will induce coupling of the nanoparticles, which shifts the LSPR frequency to that of a coupled-nanoparticle system [146]. Gold spherical particles that aggregate or assemble into close-packed structures have displayed strong LSPR red shifts [151,152]. This red shift is attributed to the formation of favorable coupled plasmon oscillation modes, which require lower energy excitation to drive the oscillation. As the inter-particle distances decrease in size, the neighboring electric fields experienced by each particle are strengthened, causing the LSPR wavelength to red shift [148,151,153]. Noble metal nanoparticle pairs lithographically fabricated with exact inter-particle separation have shown that the red-shift in the plasmon resonance wavelength increases exponentially with decreasing nanoparticle separation [148,151,153]. The coupling strength of neighboring nanoparticles exponentially decays over a distance of ~0.2 times the particle diameter [146]. Nanoparticle composition will specify the ultimate strength of the plasmonic fields; however, the decay distance will remain

independent of the composition. Shape and complexity of the nanoparticle will alter the decay distance and plasmonic field strength [154].

3.2 Experimental Section

3.2.1 Materials

1-Octanethiol, 1-decanethiol, 1-dodecanethiol, 1-octadecanethiol, 1,8-octanedithiol, and 1,6-hexanedithiol were purchased from Sigma-Aldrich. (3-Aminopropyl)triethoxysilane (APTES), (3-mercaptopropyl)triethoxysilane, and p-terphenyl-4,4″-dithiol were purchased from Sigma-Aldrich. All solvents were used as purchased from Fisher Aldrich. Water used in this work was purified using a Millipak Express, where particulate matter was removed via a 0.22 μm filter. Sapphire prisms were purchased from Meller Optics, Inc. All glassware was cleaned using aqua regia and generously rinsed before use.

3.2.2 Sapphire Prism Preparation

Planar surfaces are a common substrate for both SAM and nanoparticle deposition due to the compatibility of the sample structure with various surface analysis techniques including, X-ray photoelectron spectroscopy (XPS), scanning probe microscopies (SPM), scanning electron microscopy (SEM), among others [155-159,160]. The most common planar substrates for SAMs formed from alkanethiols are thin metallic films formed on mica and silicon wafers [157]. Such substrates are formed through physical vapor deposition (PVD), electrodeposition, or electroless deposition [161-163]. Although gold is the favored film deposited, other metals including silver, palladium, copper, platinum, and alloys can be used to prepare thin films on planar substrates. Applications that focus on measurements of electron transport through sulfur terminated molecules benefit greatly from substrates that are single crystal, or polycrystalline with large

grains [157]. Gold is favored over similar metals for its lower melting point. At comparable deposition rates, metals with higher melting points, such as palladium (1552 °C) and platinum (1772 °C) produce smaller grains when compared to gold (1064 °C). [165] Gold thin films are also relatively inert, allowing for atmospheric measurements at temperatures up to the melting temperature. In addition, gold exhibits a high alkanethiol binding affinity, allowing for SAM formation that remains stable for days to weeks [157]. A common substrate used in STM analysis is freshly cleaved mica supporting gold thin films. Gold is deposited epitaxially onto the nearly atomically flat (100) mica surface, forming thin films strongly (111) oriented [166,167].

Transferring atomically flat (111) gold thin films onto the sapphire prisms necessary for photon STM analysis necessitates additional processing. Sapphire substrates with various crystallographic surfaces can be purchased commercially [168]. In this work sapphire substrates bearing a (0001) plane (Meller Optics Inc.) were purchased and thermally annealed to obtain atomically flat, wide atomic planes. AFM images of sapphire prisms annealed for 24 hours at 1500 °C and 18 hours at 1400 °C (Figure 3.2). Following annealing a 2 nm thick Nb seed layer was evaporated at a rate of 0.015 nm/s at room temperature. A thin 40 nm gold film was then deposited at a temperature of 500 °C at a rate of 0.05 nm/s. A final thermal sequence of 24 hours at 500 °C and 18 hours at 400 °C was then performed. Thermal annealing of the metal films induces grain boundary migration (Figure 3.3), creating larger grains and wider terraces [169].

3.2.3 Nanoparticle Deposition

Determining a method of depositing nanoparticles onto substrates suitable for STM analysis is a unique challenge for this analysis method. Procedures to deposit nanoparticles onto gold layers evaporated on mica substrates and sapphire substrates while maintaining the integrity

of deposited nanoprisms has proven particularly challenging. Initial deposition techniques involved direct application of a range of concentrations of nanoprism solutions directly to the gold surface. Previous studies have applied solutions via direct deposition or spin coating [161-163]. Replication of these methods resulted in low concentration, highly dispersed nanoprisms dominating a majority of the sample area with select regions of multilayered, nanoprism aggregates in the case of direct deposition (Figure 3.4). Initial alterations to this method included applying nanoprism solutions of higher concentrations, deposition onto heated substrates expediting solution evaporation, and sonication of samples after highly concentrated depositions or multiple deposition applications. Although each alteration resulted in more favorable dispersions, none resulted in conditions conducive to scanning.

Deposition of the nanoparticles to gold film covered surfaces at first seems trivial in application. Reproducibly creating densely packed monolayers while maintaining long range (mm) dispersion homogeneity requires strict control of the nanoparticle functionalization, functionalization of the gold substrate, and careful selection of the medium in which the solution is deposited. These key factors enable the direct control of nanoparticle concentration and physical deposition method that traditionally control the nanoparticle deposition density.

3.2.3 Ligand Substitution

The nanoprisms used in this work follow the synthesis method detailed in the second chapter of this thesis. As such, the starting nanoprisms are functionalized with a protective ligand of CTAB. Final analysis of these particles necessitates the exchange of CTAB with 1-dodecanethiol protective layers. Several studies have been conducted concerning ligand substitution of gold nanoparticles [173,174]. Substitution of nanoparticles with rod length or

edge length over 100 nm have been successful; however, irreversible aggregation is common. Slightly smaller particles of edge lengths under 50 nm have successfully undergone substitution of charge bound salts to several *n*-alkanethiol species. Although several extensive methods have been suggested in previous works, a simple procedure was developed to exchange the ligand coating on the nanoprisms [173,174]. A 1.5 mL solution of as-prepared nanoprisms was precipitated via centrifugation and dispersed in a 0.1 mL 10 mM CTAB solution. This solution was then added to 0.1 mL of the desired *n*-alkanethiol. In this work 1,8-octanedithiol and 1,12-dodecanethiol were used. A single drop of acetone was then added to the solution at which point the solution was vigorously shaken. Acetone has been shown to weaken the bonding of CTAB to gold nanoparticle surfaces [175]. The solution was then sonicated for up to 30 seconds to achieve complete dispersion. Over five minutes the solution separates into aqueous and alkanethiol solutions. The alkanethiol portion, which is green in color due to high nanoprism concentration, is then removed and diluted with ethanol, as desired. Ligand substitution enabled the suspension of nanoprisms in other solvents. *n*-Alkanethiol functionalized nanoprisms were deposited in polar, "borderline" polar, and non-polar solvents with limited ranges of success. It was found that using non-polar solvents, particularly toluene, yielded the most optimized distribution of nanoprisms (Figure 3.5).

In addition to modifying the nanoprism protective ligand, the gold surface has also been functionalized to minimize nanoprism migration once deposited on the surface, yet still suspended in the deposition solvent. 1,6-Hexadecanedithiol and 1,8-octadecanedithiol were used to functionalize the substrate surface solution deposition. To ascertain the effectiveness of alkanedithiol functionalization via microcontact printing (μCP) was utilized to create both the control and functionalized surfaces simultaneously. This type of patterning uses flexible,

patterned PDMS reliefs that have been submerged in an alkanethiol solution which acts as the "ink". Once the stamp has dried it is pressed against the ethanol wetted gold substrate. The alkanethiols then transfer from the stamp to the substrate as determined by the stamping pattern. The remaining non-functionalized areas surrounding the alkanethiol pattern are then backfilled using the corresponding alkanedithiol. Nanoprism solutions using direct deposition have shown that applied nanoprisms preferentially adsorb to the alkanedithiol patterned regions. (Figure 3.6) Nanoparticles were also applied using μCP. Substituting nanoparticle solutions for the "ink," nanoprisms were deposited onto a wetted gold substrate (Figure 3.7) In addition to direct deposition; solution deposition and spin coating were used to deposit nanoprisms onto the gold surface. Direct deposition resulted in a particle surface density closer to that needed for STM analysis. (Figure 3.8a) Subsequent exploration of alternate molecules to functionalize the surface found that p-terphenyl-4,4"-dithiol (TPDT) yielded an optimal dispersion of nanoprisms. (Figure 3.8b)

3.2.1 Surface Nanoparticle Purification and Functionalization

Single-particle characterizations have been achieved using several types of SPM [176,178]. Single-molecule investigations produced via molecular insertion rely on precise control of relative molecular electronic states and molecular heights. Previous work exploring surface-bound, photonically induced reactions of single molecules depends upon complete knowledge of each species of molecule present in order to attribute the features observed to specific molecules [49]. The presence of contaminants complicates precise molecular identification, in addition to disrupting the order of the alkanethiol SAM.

Specific control of the molecular systems deposited on gold nanoprisms is essential to extract significant information during STM analysis. Control of the adsorbed monolayer that

surrounds and restricts the motion of inserted molecules of interest enables the identification and characterization of inserted molecules. Residual CTAB adsorbed to the nanoprism surface do not form ordered monolayers and as such are not conducive to molecular insertion or STM analysis [32,176]. Previous studies removed citrate ligands by submersion in solutions of alkanethiol dispersed in ethanol [176]. Techniques to remove CTAB are substantially difficult, generally using aggressive corrosives [177]. Such processes which use piranha solution (H_2O_2-H_2SO_4 = 1:3, v/v) caused immediate particle ripening due to the high surface density of nanoparticles. The process developed used a brief rinse of deionized water followed by brief rinse using acetone. Flame annealing can remove contaminants from the surface of gold films and proved effective in significantly reducing CTAB remaining on the gold nanoprisms in addition to removing reaming TPDT adsorbed on the gold film surface. The entire sample then underwent solution deposition of 1 μM 12-dodecanethiol depositing a monolayer on both the nanoprisms and gold film substrate.

3.2 Results and Discussion

Alkanethiol-functionalized gold nanoprism samples were analyzed using photon STM operating under ambient conditions. Nanoprisms were initially located using large, 1500 Å x 1500 Å low-resolution scans. The tip was then moved directly over the nanoprism at which point subsequent high-resolution, scans (1000 Å x 1000 Å and less) were recorded. Initial images were taken over several areas as nanoprisms were observed. Tip integrity deteriorated quickly, lasting up to the collection of 10 images, due to underlying sample surface roughness inhibiting reproducible and conclusive data collection. During the cleaning of the sapphire prisms used for this work the planar surface quality unexpectedly decreased, causing a greater roughening of the scanning surface. Nanoprisms were imaged using STM (Figure 3.9) although subsequent

high-resolution scans were inhibited due to tip degradation and sample quality. Protrusions were observed on the surface of the nanoprisms, which are attributed to residual CTAB adsorbed to the surface (Figure 3.10). It is expected that increased stringency of the surface nanoparticle functionalization and replacement of the sapphire prisms will produce molecular resolution of alkanethiolate SAMs deposited on nanoprisms.

3.4 Conclusions and Future Prospects

The development of a deposition method of the prepared nanoprisms proved challenging in reproducibly creating large areas of highly packed single monolayer nanoprisms. Several approaches that were applied in previous work yielded low density nanoprism deposition [176,177]. Spin coating and solution deposition yielded highly dispersed nanoprisms that were not amenable to STM analysis. Application of TPDT functionalization proved to be the most influential variable in nanoprism deposition. Ligand substitution and selection of solvent did not greatly alter the particle density when applied to a TPDT functionalized substrate. Optimal deposition was attained using as synthesized CTAB protected nanoprisms deposited on TPDT-functionalized surfaces using acetone added to the aqueous CTAB nanoprism solution.

In this work, nanoprisms on gold film substrates have been demonstrated as viable systems for high-resolution photon STM analysis. Aggressive protective ligands that have previously proven inhibitive in producing ordered alkane SAM have been removed and initial nanoprism images have been ascertained. Although single-molecule measurements have not been attained in this work, sufficient groundwork has been developed to analyze such systems in the near future.

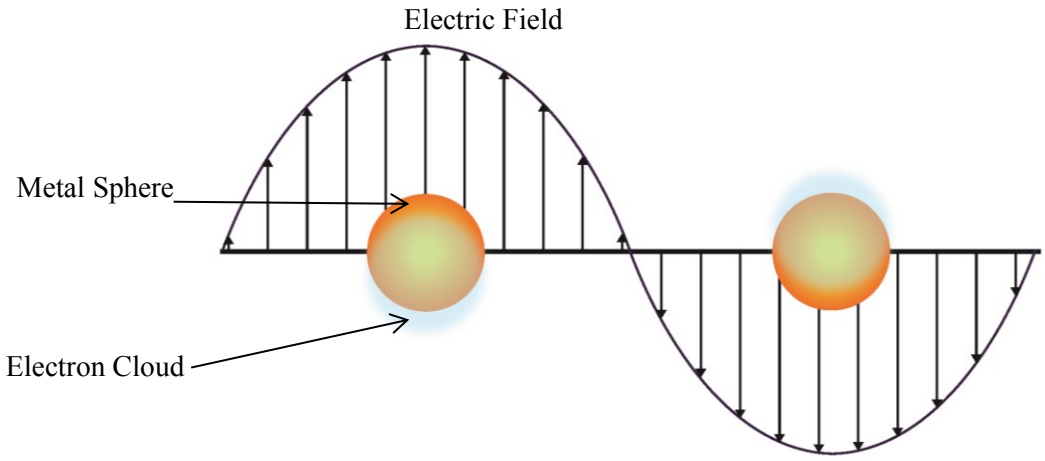

Figure 3.1: Schematic of local surface plasmon resonance depicting the oscillation of the electron cloud of a metal nanoparticle due to strong coupling with incident light.

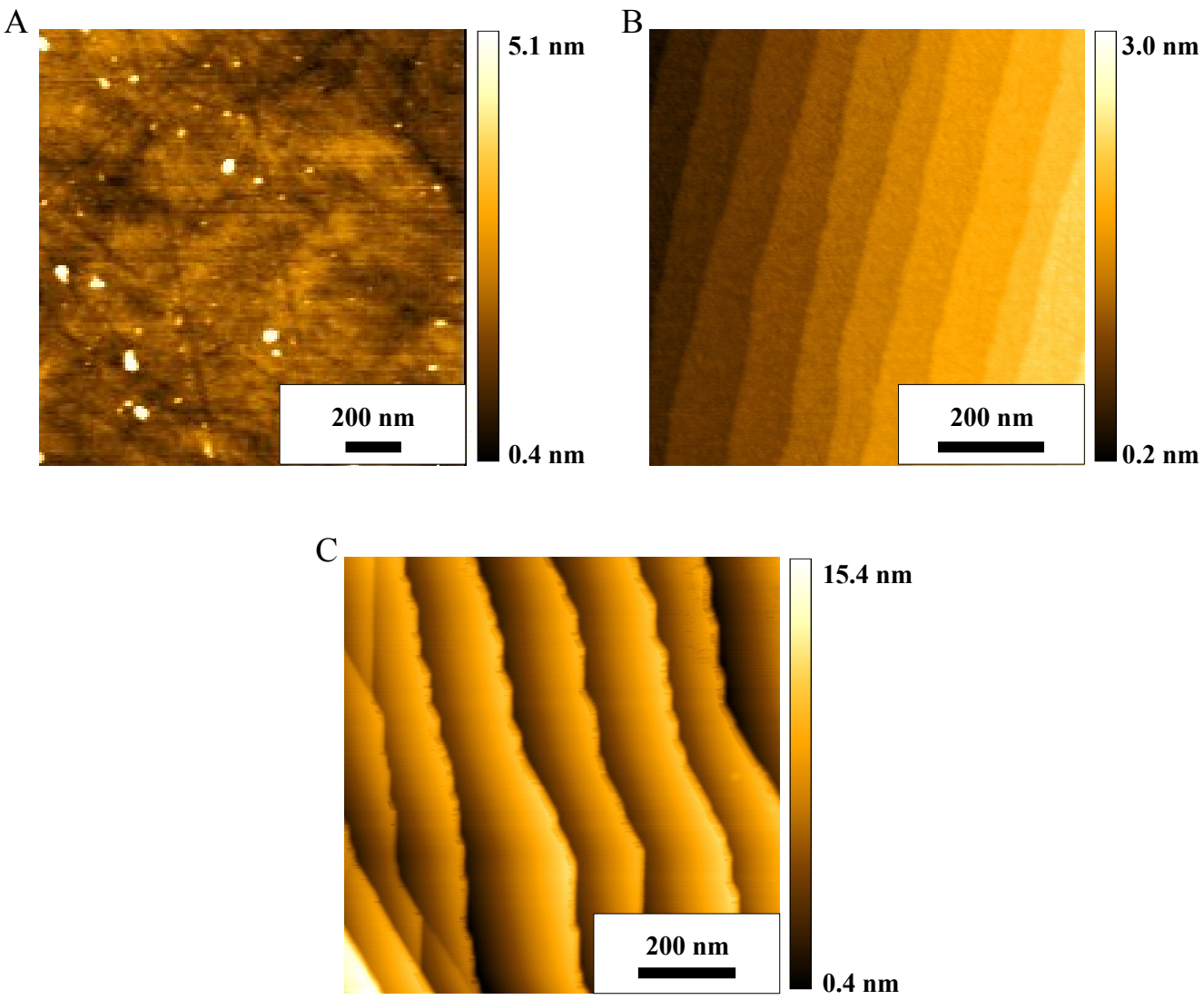

Figure 3.2: Atomic force microscopy image of the planar surface of an epitaxially polished, c-cut sapphire prism. (**A**) The surface as purchased, (**B**) after 24 hours of annealing at 1400 °C, (**C**) and after an additional 24 hours of annealing at 1500 °C.

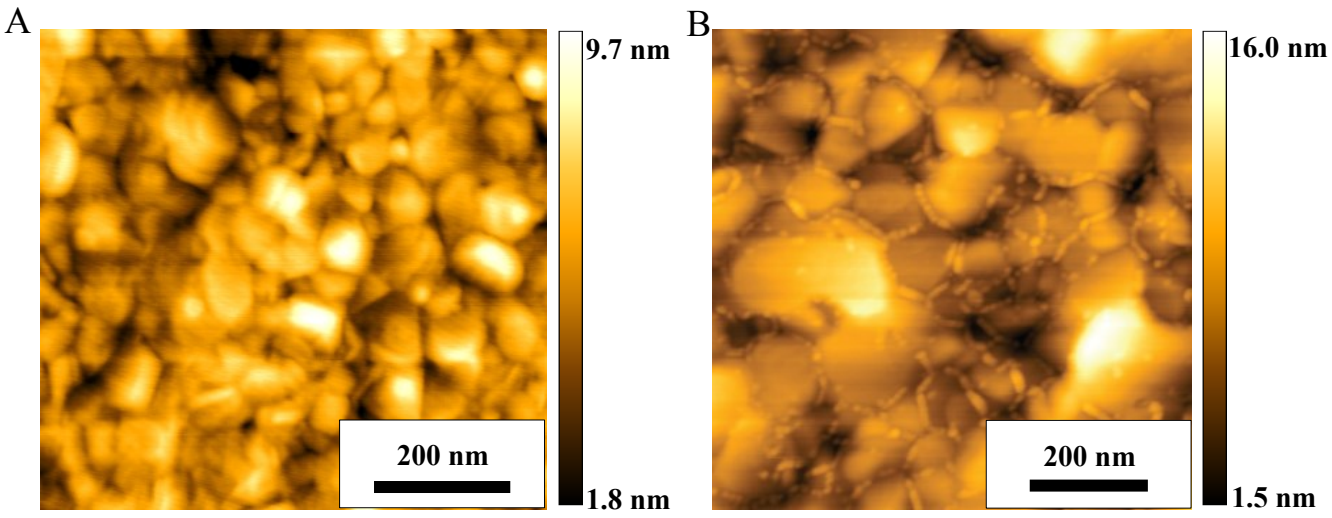

Figure 3.3: Atomic force microscopy image of a gold film evaporated onto the planar surface of a sapphire prism. (**A**) The gold surface directly after evaporation. (**B**) The gold surface after a thermal annealing sequence of 24 hours at 500 °C followed by an additional 18 hours of annealing at 400 °C.

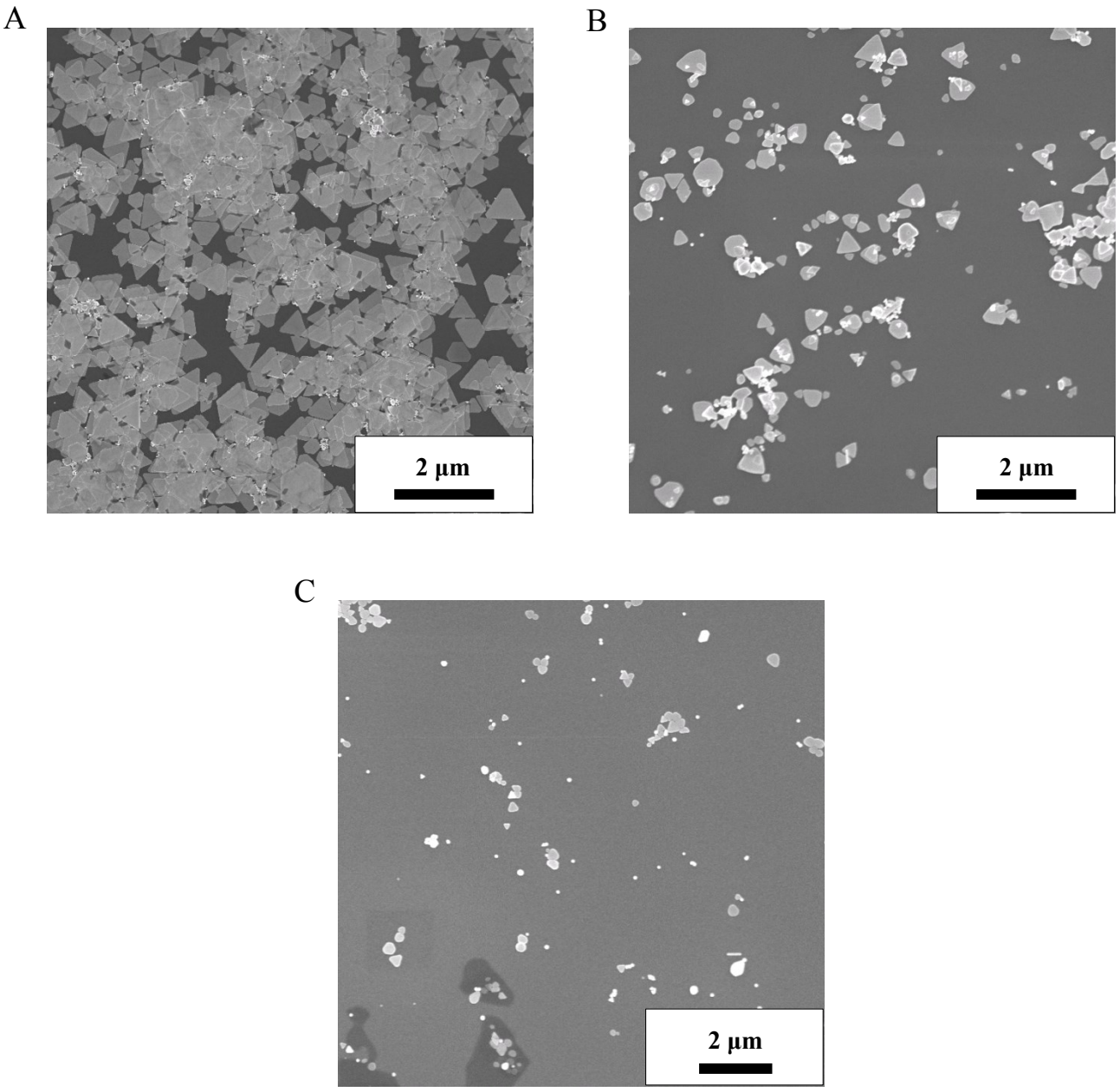

Figure 3.4: Scanning electron microscopy images of nanoprisms deposited onto silicon wafer substrates. After selected application any remaining solution evaporated naturally and the sample was prepared for analysis. (**A**) Direct deposition of nanoprism solution to the substrate surface. (**B**) Spin-coat deposition of nanoprism solution to the substrate surface. (**C**) Submersion of the substrate in nanoprism solution.

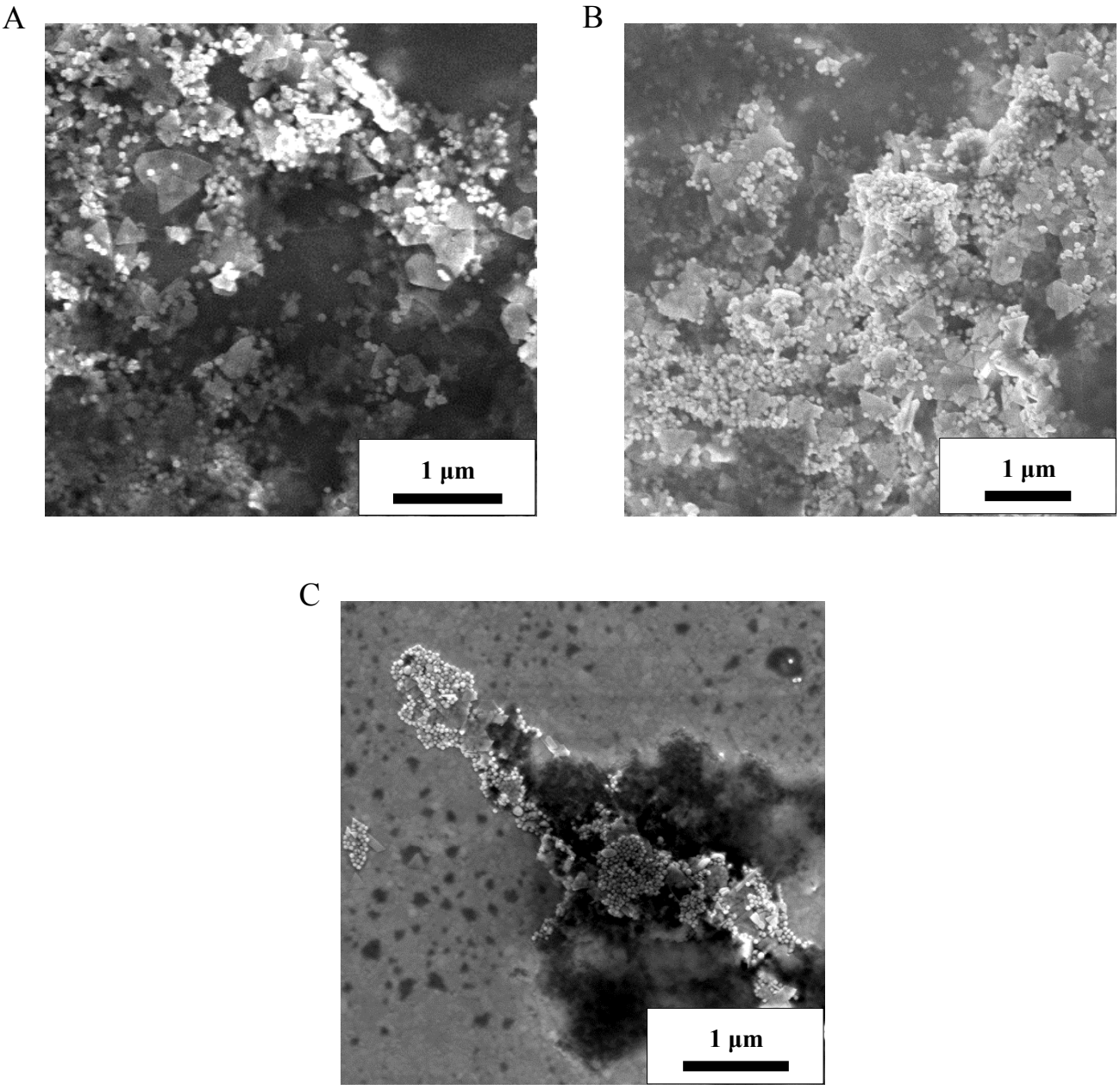

Figure 3.5: Scanning electron microscopy images of 1-octanedithiol-stabilized nanoprisms deposited onto gold-coated silicon wafer substrates. (**A**) Nanoprisms suspended in toluene. (**B**) Nanoprisms suspended in hexane. (**C**) Nanoprisms suspended in ethanol. Nanoprism solutions were directly applied to the substrate and allowed to dry in air and prepared for analysis.

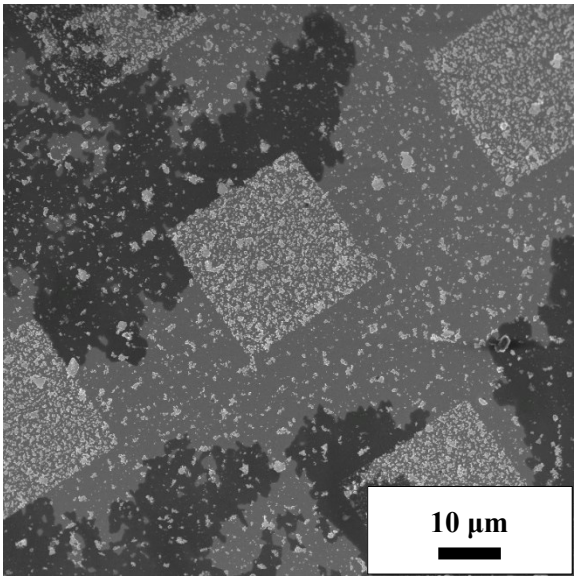

Figure 3.6: SEM image of nanoprisms deposited onto gold-coated silicon wafer substrates. Substrates were prepared using microcontact printing to pattern 25 µm x 25 µm squares of bare gold in a 1-octanethiol grid. The bare squares were then backfilled with 1,8-octanedithiol. Nanoprism solution was then directly deposited and allowed to dry.

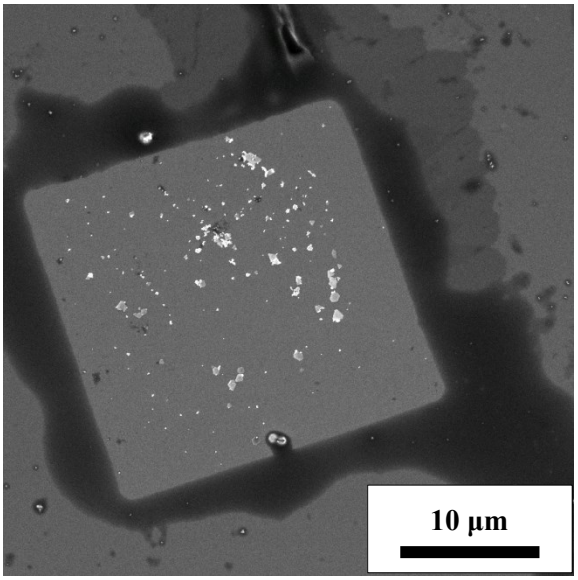

Figure 3.7: Scanning electron microscopy image of nanoprisms stamped onto gold-coated silicon wafer substrates. After printing the sample dried in air and prepared for analysis.

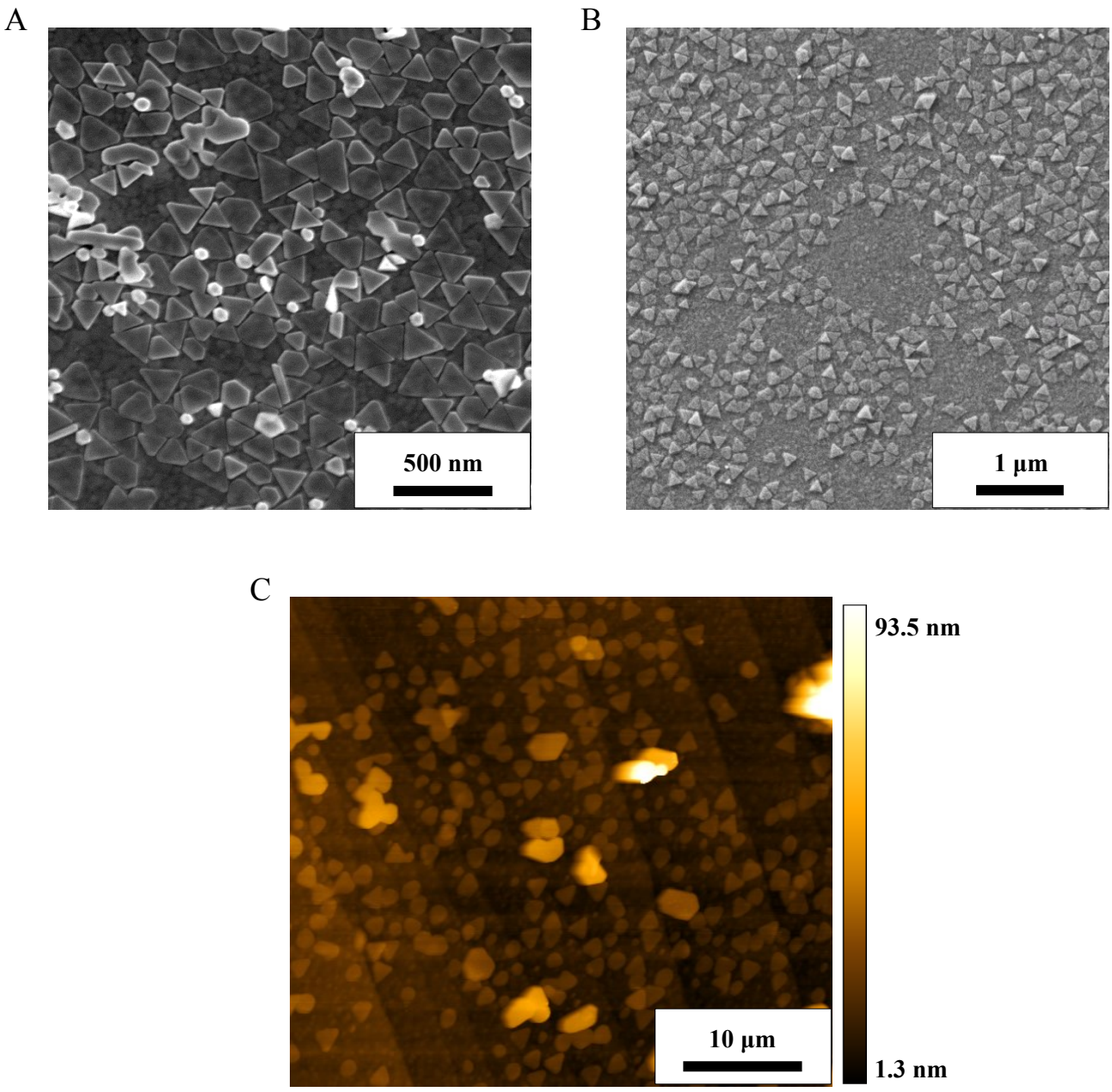

Figure 3.8: Scanning electron microscopy images of nanoprisms deposited onto: (**A**) gold-coated silicon wafer functionalized with 1,8-octanedithiol. (**B**) Gold-coated silicon wafer functionalized with TPDT. (**C**) Gold-coated sapphire prism functionalized with TPDT. Nanoprism deposition solutions were directly applied to the substrate and allowed to dry in air.

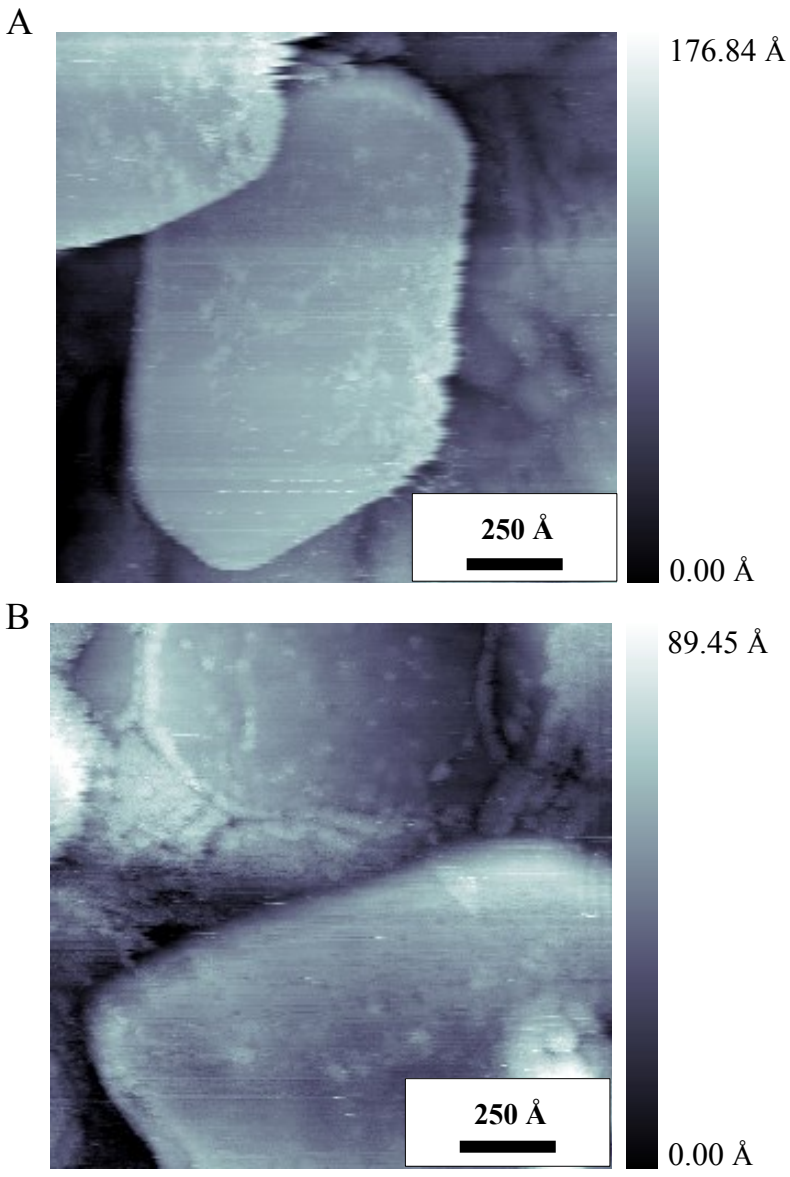

Figure 3.9: Scanning tunneling microscopy images of dodecanethiolate SAM assembled on gold nanoprisms. Tip and image degradation occurred rapidly during large scan areas of 1500 Å x 1500 Å. (**A**) Image is recorded with a sample bias (V_S) = -1 V and tunneling current (I_T) = 1 pA. (**B**) Image is recorded with V_S = -1 V and I_T = 1.95 pA.

A

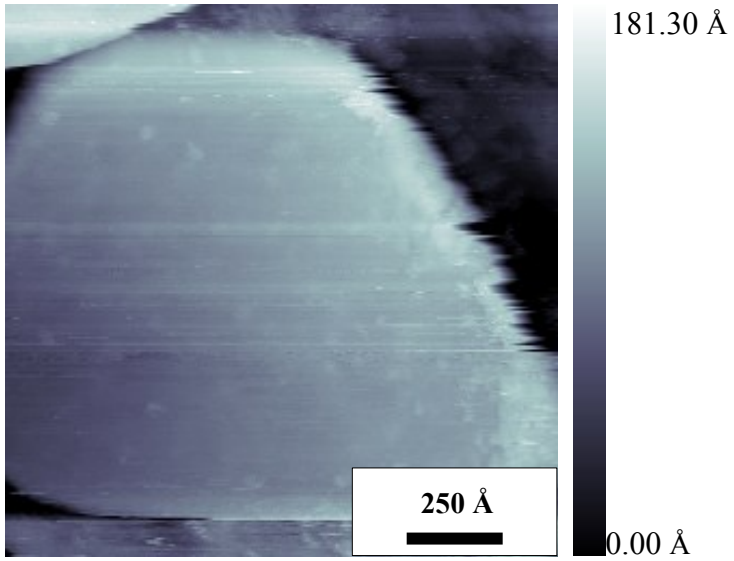

B

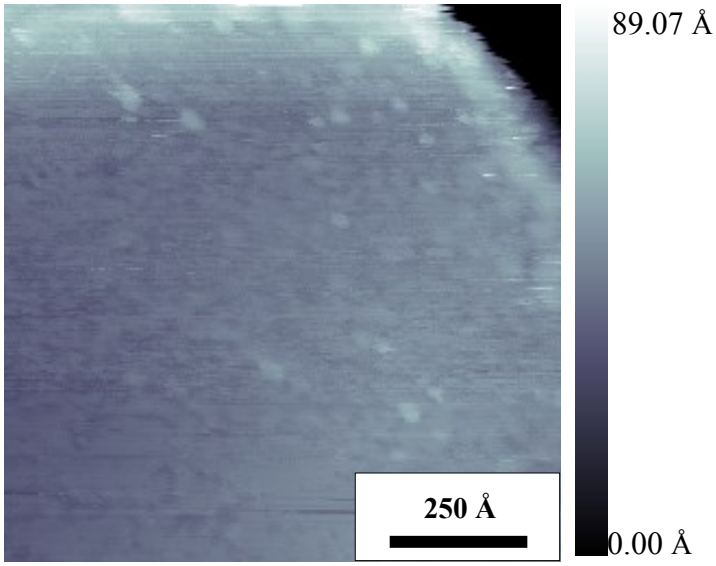

C

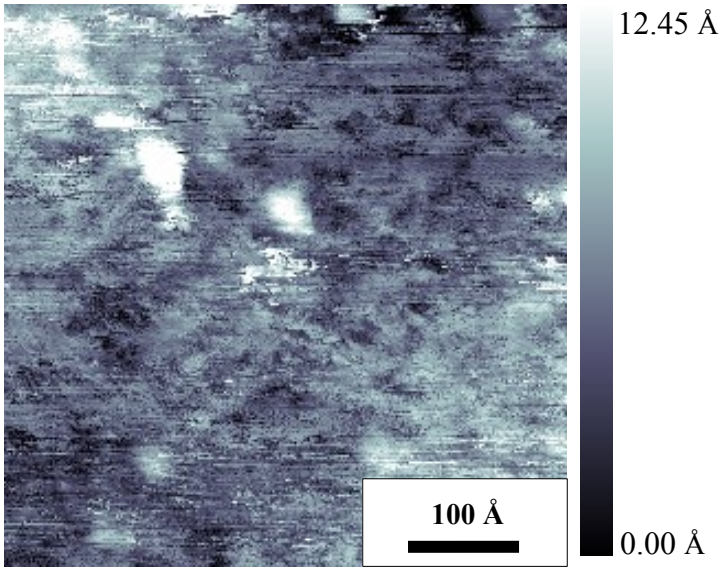

Figure 3.10: Scanning tunneling microscopy images of dodecanethiolate SAM assembled on gold nanoprisms. Each image was recorded over the same nanoprism with V_S = -1 V and I_T = 1 pA. (**A**) Image size 1000 Å x 1000 Å (**B**) Image size 1500 Å x 1500 Å. (**C**) Image size 500 Å x 500 Å.

Bibliography

Chapter 1

[1] C. J. Brabec, N. S. Sariciftci, and J. C. Hummelen, *Plastic Solar Cells*, Advanced Functional Materials **11**, 15-25 (2001)

[2] P. Peumans, A. Yakimov, and S. R. Forrest, *Small Molecular Weight Organic Thin-Film Photodetectors and Solar Cells*, Journal of Applied Physics **93**, 3693-3723 (2003)

[3] P. V. Kamat, *Photophysical, Photochemical and Photocatalytic Aspects of Metal Nanoparticles*, Journal of Physical Chemistry B **106**, 7729-7744 (2002)

[4] H. Hoppe and N. S. Sariciftci, *Morphology of Polymer/Fullerene Bulk Heterojunction Solar Cells*, Journal of Materials Chemistry **16**, 45-61 (2006)

[5] K. Zhu, N. R. Neale, A. Miedaner, and A. J. Frank, *Enhanced Charge-Collection Efficiencies and Light Scattering in Dye-Sensitized Solar Cells Using Oriented TiO_2 Nanotube Arrays*, Nano Letters **7**, 69-74 (2007)

[6] D. V. Talapin, J. S. Lee, M. V. Kovalenko, and E. V. Shevchenko, *Prospects of Colloidal Nanocrystals for Electronic and Optoelectronic Applications*, Chemical Reviews **110**, 389-458 (2010)

[7] H. Sirringhaus, P. J. Brown, R. H. Friend, M. M. Nielsen, K. Bechgaard, B. M. W. Langeveld-Voss, A. J. H. Spiering, R. A. J. Janssen, E. W. Meijer, P. Herwig, and D. M. de Leeuw, *Two-Dimensional Charge Transport in Self-Organized, High-Mobility Conjugated Polymers*, Nature **401**, 685-688 (1999)

[8] F. Gao, Y. Wang, J. Zhang, D. Shi, M. Wag, R. Humphry-Baker, P. Wang, S. M. Zakeeruddin, and M. Grätzel, A New Heteroleptic Ruthenium Sensitizer Enhances the Absorptivity of Mesoporous, *Titania Film for a High Efficiency Dye-Sensitized Solar Cell,* Chemical Communications **23**, 2635-2637 (2008)

[9] J. Burschka, N. Pellet, S. J. Moon, R. Humphry-Baker, P. Gao, M. K Nazeeruddin, and M. Grätzel, *Sequential Deposition as a Route to High-Performance Perovskite-Sensitized Solar Cells*, Nature **499**, 316-319 (2013)

[10] J. Zhao, A. Wang, and M. A. Green, *24.5% Efficiency Silicon PERT Cells on MCZ Substrates and 24.7% Efficiency PERL Cells on FZ Substrates*, Progress in Photovoltaics **7**, 471-474 (1999)

[11] S. R. Forrest, *The Limits to Organic Photovoltaic Cell Efficiency*, Materials Research Society Bulletin **30**, 28-32 (2005)

[12] A. Yella, H. W. Lee, H. N. Tsao, C Yi, A. K. Chandiran, K. Nazeeruddin, E. W. G. Diau, C. Y. Yeh, S. M. Zakeeruddin, and M. Grätzel, *Porphyrin-Sensitized Solar Cells with Cobalt (II/III)-Based Redox Electrolyte Exceed 12 Percent Efficiency*, Science **334**, 629-634 (2011)

[13] S. Y. Huang, G. Schlichthorl, A. J. Nozik, M. Gratzel, and A. J. Frank, *Charge Recombination in Dye-Sensitized Nanocrsytalline TiO_2 Solar Cells*, Journal of Physical Chemistry B **101**, 2576-2582 (1997)

[14] Y. Liang, Z. Xu, J. Xia, S. T. Tsai, Y. Wu, G. Li, C. Ray, and L. Yu, *For the Bright Future—Bulk Heterojunction Polymer Solar Cells with Power Conversion Efficiency of 7.4%*, Advanced Materials **22**, E135-E138 (2010)

[15] P. L. T. Boudreault, A. Najari, and M. Leclerc, *Processable Low-Bandgap Polymers for Photovoltaic Applications*, Chemistry of Materials **23**, 456-469 (2011)

[16] I. Robel, V. Subramanian, M. Kuno, and P. V. Kamat, *Quantum Dot Solar Cells. Harvesting Light Energy with CdSe Nanocrystals Molecularly Linked to Mesocopic TiO_2 Films*, Journal of the American Chemical Society **128**, 2385-2393 (2006)

[17] T. Hasobe, H. Imahori, P. V. Kamat, T. K. Ahn, S. K. Kim, D. Kim, A. Fujimoto, T. Hirakawa, and S. Fukuzumi, *Photovoltaic Cells Using Composite Nanocluster of Porphyrins and Fullerenes with Gold Nanoparticles*, Journal of the American Chemical Society **127**, 1216-1228 (2005)

[18] S. S. Kim, S. I. Na, J. Jo, D. Y. Kim, and Y. C. Nah, *Plasmon Enhanced Performance of Organic Solar Cells Using Electrodeposited Ag Nanoparticles*, Applied Physics Letters **93**, 073307 (2008)

[19] C. Winder and N. S. Sariciftci, *Low Bandgap Polymers for Photon Harvesting in Bulk Heterojunction Solar Cells*, Journal of Materials Chemistry **14**, 1077-1086 (2004)

[20] A. J. Morfa, K. L. Rowlen, T. H. Reilly, M. J. Romero, and J. V. Lagermaat, *Plasmon-Enhnaced Solar Energy Conversion in Organic Bulk Heterojunction Photovoltaics*, Applied Physics Letters **92**, 013504 (2008)

[21] J. Y. Kim, S. H. Kim, H. H. Lee, K. Lee, W. Ma, X. Gong, and A. J. Heeger, *New Architecture for High-Efficiency Poymer Photovoltaic Cells Using Solution-Based Titanium Oxide as an Optical Spacer*, Advanced Materials **5**, 572-576 (2006)

[22] C. Cocoyer, L. Rocha, L. Sicot, B. Geffroy, R. De Bettignies, C. Sentein, C. Fiorini-Debuisschert, and P. Raimond, *Implementation of Submicrometric Periodic Surface Structures Toward Improvement of Organic-Solar-Cell Performances*, Applied Physics Letters **88**, 133108 (2008)

[23] R. Elghanian, J. J. Storhoff, R. C. Mucic, R. L. Letsinger, and C. A. Mirkin, *Selective Colorimetric Detection of Polynucleotides Based on the Distance-Dependent Optical Properties of Gold Nanoparticles*, Science **277**, 1078-1079 (1997)

[24] J. N. Anker, W. P. Hall, O. Lyandres, N. C. Shah, J. Zhao, and R. P. Van Duyne, *Biosensing with Plasmonic Nanosensors*, Nature Materials **7**, 442-453 (2008)

[24] L. He, M. D. Musick, S. R. Nicewarmer, F. G. Salinas, S. J. Benkovic, M. J. Natan, and C. D. Keating, *Colloidal Au-Enhanced Surface Plasmon Resonance for Ultrasensitive Detection of DNA Hybridization*, Journal of the American Chemical Society **122**, 9071-9077 (2000)

[25] Y. C. Nah, S. S. Kim, J. H. Park, and D. Y. Kim, *Electrochromic Coloration of MEH-PPV Films by Electrodeposited Au Nanoparticles*, Electrochemical and Solid-State Letters **10**, J12-J14 (2007)

[26] S. Link and M. A. El-Sayed, *Shape and Size Dependence of Radiative, Non-Radiative and Photothermal Properties of Gold Nanocrystals*, International Reviews in Physical Chemistry **19**, 409-453 (2000)

[27] P. Anger, P. Bharadwaj, and L. Novotny, *Enhancement and Quenching of Single-Molecule Fluorescence*, Physical Review Letters **96**, 113002 (2006)

[28] K. L. Kelly, E. Coronado, L. L. Zhao, and G. C. Schatz, *The Optical Properties of Metal Nanoparticles: The Influence of Size, Shape, and Dielectric Environment*, Journal of Physical Chemistry B **107**, 668-677 (2003)

[29] R. C. Jin, Y. W. Cao, C. A. Mirkin, K. L. Kelly, G. C. Schatz, and J. G. Zheng, *Photoinduced Conversion of Silver Nanospheres to Nanoprisms*, Science **294**, 1901-1903 (2001)

[30] M. Grzelczak, J. Perez-Juste, P. Mulvaney, and L. M. Liz-Marzan, *Shape Control in Gold Nanoparticle Synthesis*, Chemical Society Reviews **37**, 1783-1791 (2008)

[31] W. Biglow, D. Pickett, and W. Zisman, *Oleophobic Monolayers. I. Films Adsorbed from Solution in Non-Polar Liquids*, Journal of Colloid and Interface Science **1**, 513-538 (1998)

[32] J. C. Love, L. A. Estroff, J. K. Kriebel, R. G. Nuzzo, and G. M. Whitesides, *Self-Assembled Monolayers of Thiolates on Metals as a Form of Nanotechnology*, Chemical Reviews **105**, 1103-1169 (2005)

[33] J. N. Hohman, M. Kim, B. Schüpbach, M. Kind, J. C. Thomas, A. Terfort, and P. S. Weiss, *Dynamic Double Lattice of 1-Adamantaneselenolate Self-Assembled Monolayers on Au{111}*, Journal of the American Chemical Society **133**, 19422-19431 (2011)

[34] R. G. Nuzzo and D. L. Allara, *Adsorption of Bifunctional Organic Disulfides on Gold Surfaces*, Journal of the American Chemical Society **105**, 4481-4483 (1983)

[35] R. G. Nuzzo, L. H. Dubois, and D. L. Allara, *Fundamental-Studies of Microscopic Wetting on Organic-Surfaces. 1. Formation and Structural Characterization of a Self-Consistent Series of Polyfunctional Organic Monolayers*, Journal of American Chemical Society **112**, 558-569 (1990)

[36] R. G. Nuzzo, B. R. Zegarski, and L. H. Dubois, *Fundamental-Studies of the Chemisorption of Organosulfur Compounds on Au(111) – Implications for Molecular Self-Assembly on Gold Surfaces*, Journal of American Chemical Society **109**, 733-740 (1987)

[37] B. K. Pathem, Y. B. Zheng, S. Morton, M. Å. Petersen, Y. Zhao, C. H. Chung, Y. Yang, L. Jensen, M. B. Nielsen, P. S. Weiss, *Photoreaction of Matrix-Isolated Dihydroazulene-Functionalized Molecules on Au{111}*, Nano Letters **13**, 337-343 (2013)

[38] X. Ma, Y. Guo, T. Wang, Z. Su, *Scanning Tunneling Microscopy Investigation of Self-Assembled Poly(3-hexylthiophene) Monolayer*, Journal of Chemical Physics **139**, 014701 (2013)

[39] P. Han, A. R. Kurland, A. N. Giordano, S. U. Nanayakkara, M. M. Blake, C. M. Pochas, and P. S. Weiss, *Heads and Tails: Simultaneous Exposed and Buried Interface Imaging of Monolayers*, ACS Nano **3**, 3115-3121 (2009)

[40] M. D. Porter, T. B. Bright, D. L. Allara, and C. E. D. Chidsey, *Spontaneously Organized Molecular Assemblies. 4. Structural Characterization of Normal-Alkyl Thiol Monolayers on Gold by Optical Ellipsometry, Infrared-Spectroscopy, and Electrochemistry*, Journal of the American Chemical Society **109**, 3559-3568

[41] S. V. Atre, B. Liedberg, and D. L. Allara, *Chain-Length Dependence of the Structure and Wetting Properties in Binary Composition Monolayers of OH-Terminated and CH_3-Terminated Alkanethiolates on Gold,* Langmuir **11**, 3882-3893 (1995)

[42] D. L. Allara and R. G. Nuzzo, *Spontaneously Organized Molecular Assemblies. 1. Formation, Dynamics, and Physical-Properties of Normal-Alkanoic Acids Adsorbed from Solution on an oxidized Aluminum Surface*, Langmuir **1**, 45-52 (1985)

[43] D. L. Allara and R. G. Nuzzo, *Spontaneously Organized Molecular Assemblies. 2. Quantitative Infrared Spectroscopic Determination of Equilibrium structures of Solution-Adsorbed normal-Alkanoic Acids on an Oxidized Aluminum Surface*, Langmuir **1**, 52-66 (1985)

[44] G. E. Poirier, *Characterization of Organosulfur Molecular Monolayers on Au(111) Using Scanning Tunneling Microscopy*, Chemical Reviews **97***, 1117-1127 (1997)*

[45] G. E. Poirier and M. J. Tarlov, *The c(4x2) Superlatice of n-Alkanethiol Monolayers Self-Assembled on Au(111)*, Langmuir **10**, 2853-2856 (1994)

[46] G. E. Poirier and E. D. Pylant, *The Self-Assembly Mechanism of Alkanethiols on Au(111)*, Science **272**, 1145-1148 (1994)

[47] G. E. Poirier, *Mechanism of Formation of Au Vacancy Islands in Alkanethiol Monolayers on Au(111)*, Langmuir **13**, 2019-2026 (1997)

[48] L. A. Bumm, J. J. Arnold, M. T. Cygan, T. D. Dunbar, T. P. Burgin, L. Jones, D. L. Allara, J. M. Tour, and P. S. Weiss, *Are Single Molecular Wires Conducting?*, Science **271**, 1705-1707 (1996)

[49] M. Kim, J. N. Hohman, Y. Cao, K. N. Houk, H. Ma, A. K. Y. Jen, and P. S. Weiss, *Creating Favorable Geometries for Directing Organic Photoreactions in Alkanethiolate Monolayers*, Science **331**, 1312-1315 (2011)

[50] Z. J. Donhauser, B. A. Mantooth, T. P. Pearl, K. F. Kelly, S. U. Nanayakkara, and P. S. Weiss, *Matrix-Mediated Control of Stochastic Single Molecule Conductance Switching*, Japanese Journal of Applied Physics **41**, 4871-4877(2002)

[51] A. M. Moore, B. A. Mantooth, Z. J. Donhauser, F. Maya, D. W. Price, Y. X. Yao, J. M. Tour, and P. S. Weiss, *Cross-Step Place-Exchange of Oligo(phenylene-ethynylene) Molecules*, Nano Letters **5**, 2292-2297 (2005)

[52] A. M. Moore, B. A. Mantooth, Z. J. Donhauser, Y. Yao, J. M. Tour, and P. S. Weiss, *Real-Tim Measurements of Conductance Switching and Motion of Oligo(phenylene-ethynylene)s*, Journal of the American Chemical Society **129**, 10352 (2007)

[53] A. M. Moore, A. A. Dameron, B. A. Mantooth, R. K. Smith, D. J. Fuchs, J. W. Ciszek, F. Maya, y. X. Yao, J. M. Tour, and P. S. Weiss, *Molecular Engineering and Measurements to Test Hypothesized Mechanisms in Single-Molecule Conductance Switching*, Journal of the American Chemical Society **128**, 1959-1967 (2006)

[54] G. Binnig and H. Rohrer, *Scanning Tunneling microscopy*, Helvetica Physica Acta **55**, 726-735 (1982)

[55] G. Binnig and H. Rohrer, *Scanning Tunneling Microscopy*, IBM Journal of Research and Development **30**, 355-369 (1986)

[56] G. Binnig and H. Rohrer, *Scanning Tunneling Microscopy: From Birth to Adolescence*, Reviews of Modern Physics **59**, 615-625 (1987)

[57] J. E. Griffith and G. P. Kochanski, *Scanning Tunneling Microscopy*, Annual Review of Materials Science **20**, 219-244 (1990)

[58] R. Nishitani and A. Kasuya, *STM Induced Photon Emission at the Liquid-Solid Interface*, Surface Science **433**, 283-287 (1999)

[59] D. M. Eigler, P. S. Weiss, E. K. Schweizer, and N. D. Lang, *Imaging Xe with a Low-Temperature Scanning Tunneling Microscope*, Physical Review Letters **66**, 1189-1192 (1991)

[60] J. H. Ferris, J. G. Kushmerick, J. A. Johnson, M. G. Y. Youngquist, R. B. Kessinger, H. F. Kingsbury, and P. S. Weiss, *Design, Operation, and Housing of an Ultrastable, Low Temperature, Ultrahigh Vacuum Scanning Tunneling Microscope*, Review of Scientific Instruments **69**, 2691-2695 (1998)

[61] M. A. Henderson, *The Interaction of Water with Solid Surfaces: Fundamental Aspects Revisited*, Surface Science Reports **46**, 1-308 (2002)

[62] A. O. Golubok and V. A. Timofeev, *STM Combined with SEM without SEM Capability Limitations*, Ultramicroscopy **42**, 1558-1563 (1992)

[63] D. Sawada, A. Hirai, Y. Sugimoto, M. Abe, and S. Morita, *Simultaneous Atomic Imaging of Atomic Force Microscopy and Scanning Tunneling Microscopy Using Metal Coated Cantilevers*, Materials Transactions **50**, 940-942 (2009)

[64] A. M. Moore, S. Yeganeh, Y. X. Yao, S. A. Claridge, J. M. Tour, M. A. Ratner, and P. S. Weiss, *Polarizabilities of Adsorbed and Assembled Molecules: Measuring the Conductance through Buried Contacts*, ACS Nano **4**, 7630-7636 (2010)

[65] J. Tersoff and D. R. Hamann, *Theory and Application for the Scanning Tunneling Microscope*, Physical Review Letters **50**, 1998-2001 (1983).

[66] N. Garcia, *Theory of Scanning Tunneling Microscopy and Spectroscopy – Resolution, Image and Field States, and Thin Oxide Layers*, IBM Journal of Research and Development **30**, 533-542 (1986).

[67] N. Pertaya, K. F. Braun, and K. H. Rieder, *On the Stability of Besocke-Type Scanners*, Review of Scientific Instruments **75**, 2608-2612 (2004)

[68] S. H. Pan, E. W. Hudson, and J. C. Davis, *^{3}He Refrigerator Based Very Low Temperature Scanning Tunneling Microscope*, Review of Scientific Instruments **70**, 1459-1463 (1999)

Chapter 2

[69] M. Faraday, *Experimental Relations of Gold (and Other Metals) to Light*, Philosophical Transactions **147**, 145-181 (1856)

[70] A. N. Shipway, E. Katz, and I. Willner, *Nanoparticle Arrays on Surfaces for Electronic, Optical and Sensor Applications*, ChemPhysChem **1**, 18-52 (2000)

[71] S. J. Oldenburg, R. D. Averitt, S. L. Westcott, and N. J. Halas, *Nanoengineering of Optical Resonances* **288**, 243-247 (1998)

[72] X. H. Gao, Y. Y. Cui, R. M. Levenson, L. W. K. Chung, and S. M. Nie, *In Vivo Cancer Targeting and Imaging with Semiconductor Quantum Dots*, Nature Biotechnology **22**, 969-976 (2004)

[73] C. Y. Jiang, S. Markutsya, Y. Pikus, and W. Tsukruk, *Freely Suspended Nanocomposite Membranes as Highly Sensitive Sensors*, Nature Materials **3**, 721-728 (2004)

[74] K. A. Willets, and R. P. Van Duyne, *Localized Surface Plasmon Resonance Spectroscopy and Sensing*, Annual Review of Physical Chemistry **58**, 267-297 (2007)

[75] A. R. Tao, S. Habas, and P. D. Yang, *Shape Control of Colloidal Metal Nanocrystals*, Small **4**, 310-325 (2008)

[76] F. Caruso, R. A. Caruso, and H. Mohwald, *Nanoengineering of Inorganic and Hybrid Hollow Spheres by Colloidal Templating*, Science **282**, 1111-1114 (1998)

[77] H. Hiramatsu, and F. E. Osterloh, *A Simple Large-Scale Synthesis of Nearly Monodisperse Gold and Silver Nanoparticles with Adjustable Sizes and with Exchangeable Surfactants*, Chemistry of Materials **16**, 2509-2511 (2004)

[78] J. Turkevitch, P. C. Stevenson, J. Hillier, *Nucleation and Growth Process in the Synthesis of Colloidal Gold*, Discussions of the Faraday Society **11**, 55 (1951)

[79] M. Hu, J. Chen, Z. Li, L. Au, G. V. Hartland, X. Li, M. Marquez, and Y. Xia, *Gold Nanostructures: Engineering their Plasmonic Properties for Biomedical Applications*, Chemical Society Reviews **35**, 1084-1094 (2006)

[80] T. Y. Olson and J. Z. Zhang, *Structural and Optical Properties and Emerging Applications of Metal Nanomaterials*, Journal of Material Science Technologies **24**, 433-446 (2008)

[81] J. E. Millstone, S. Park, K. L. Shuford, L. Qin, G. C. Schatz, and C. A. Mirkin, *Observation of a Quadrupole Plasmon mode for a Colloidal Solution of Gold Nanoprisms*, Journal of the American Chemical Society **127**, 5312-5313 (2005)

[82] J. E. Millstone, G. S. Metraux, and C. A. Mirkin, *Controlling the Edge Length of Gold Nanoprisms via a Seed-Mediated Approach*, Advanced Functional Materials **16**, 1209-1214 (2006)

[83] T. H. Ha, H. J. Koo, and B. H. Chung, *Shape-Controlled Syntheses of Gold Nanoprisms and Nanorods Influenced by Specific Adsorption of Halide Ions*, Journal of Physical Chemistry C **111**, 1123-1130 (2007)

[84] J. S. DuChene, W. Niu, J. M. Abendroth, Q. Sun, and W. D. Wei, *Halide Anions as Shape-Directing Agents for Obtaining High-Quality Anisotropic Gold Nanostructures*, Chemistry of Materials **25**, 1392-1399 (2013)

[85] S. C. Glotzer and M. J. Solomon, *Anisotropy of Building Blocks and their Assembly into Complex Structures*, Nature Materials **6**, 557-562 (2007)

[86] Z. Y. Tang and N. A. Kotov, *One-Dimensional Assemblies of Nanoparticles: Preparation, Properties, and Promise*, Advanced Materials **17**, 951-962 (2005)

[87] O. M. Bakr, B. H. Wunsch, and F. Stellacci, *High-Yield Synthesis of Multi-Branched Urchin-like Gold Nanoparticles*, Chemistry of Materials **18**, 3297-3301 (2006)

[88] L. Vayssieres, *Growth of Arrayed Nanorods and Nanowires of ZnO from Aqueous Solutions*, Advanced Materials **15**, 464-466 (2003)

[89] B. Liu and E. S. Aydil, *Growth of Oriented Single-Crystalline Rutile TiO_2 Nanorods on Transparent Conducting Substrates for Dye-Sensitized Solar Cells*, Journal of the American Chemical Society **131**, 3985-3990 (2009)

[90] J. A. Zhang, M. R. Langille, and C. A. Mirkin, *Photomediated Synthesis of Silver Triangular Bipyramids and Prisms: The Effect of pH and BSPP*, Journal of the American Chemical Society **132**, 12502-12510 (2010)

[91] B. Pietrobon and V. Kitaev, *Photochemical Synthesis of Monodisperse Size-Controlled Silver Decahedral Nanoparticles and Their Remarkable Optical Properties*, Chemistry of Materials **20**, 5186-5190 (2008)

[92] C. Chen, L. Wang, G. H. Jiang, and H. J. Yu, *Chemical Preparation of Special-Shaped Metal Nanomaterials through Encapsulation or Inducement in Soft Solution*, Reviews on Advanced Materials Science **11**, 1-18 (2006)

[93] R. Narayanan and M. A. El-Sayed, *Effect of Nanocatalysis in Colloidal Solution on the Tetrahedral and Cubic Nanoparticle Shape: Electron-Transfer Reaction Catalyzed by Platinum Nanoparticles*, Journal of Physical Chemistry B **108**, 5726-5733 (2004)

[94] K. K. Caswell, C. M. Bender, and C. J. Murphy, *Seedless, Surfactantless Wet Chemical Synthesis of Silver Nanowires*, Nano Letters **3**, 667-669 (2003)

[95] A. C. Templeton, M. J. Hostetler, C. T. Kraft, and R. W. Murray, *Reactivity of Monolayer-Protected Gold Cluster Molecules: Steric Effects*, Journal of the American Chemical Society **120**, 1906-1911 (1998)

[96] D. Nykypanchuk, M. M. Maye, D. van der Lelie, and O. Gang, *DNA-Guided Crystallization of Colloidal Nanoparticles*, Nature **451**, 549-552 (2008)

[97] R. Jin, Y. Cao, C. A. Mirkin, K. L. Kelly, G. C. Schatz, and J. G. Zheng, *Photoinduced Conversion of Silver Nanospheres to Nanoprisms*, Science **294**, 1901-1903 (2001)

[98] A. M. Schwartzberg, T. Y. Olson, C. E. Talley, and J. Z. Zhang, *Synthesis, Characterization, and Tunable Optical Properties of Hollow Gold Nanospheres*, Journal of Physical Chemistry B **110**, 19935-19944 (2006)

[99] S. Link and M. A. El-Sayed, *Size and Temperature Dependence of the Plasmon Absorption of Colloidal Gold Nanoparticles*, Journal of Physical Chemistry B **103**, 4212-4217 (1999)

[100] T. S. Ahmadi, S. L. Logunov, and M. A. ElSayed, *Picosecond Dynamics of Colloidal Gold Nanoparticles*, Journal of Physical Chemistry **100**, 8053-8056 (1996)

Chapter 3

[101] M. Law, L. E. Greene, J. C. Johnson, R. Saykally, and P. D. Yang, *Nanowire Dye-Sensitized Solar Cells*, Nature Materials **4**, 455-459 (2005)

[102] Z. Y. Tang, N. A. Kotov, and M. Giersig, *Spontaneous Organization of Single CdTe Nanoparticles into Luminescent Nanowires*, Science **297**, 237-240 (2002)

[103] P. V. Kamat, *Photophysical, Photochemical and Photocatalytic Aspects of Metal Nanoparticles*, Journal of Physical Chemistry B **106**, 7729-7744 (2002)

[104] R. Möller, U. Albrecht, J. Boneberg, B. Koslowski, P. Leiderer, and K. Dransfeld, *Detection of Surface Plasmons by Scanning Tunneling Microscopy*, Journal of Vacuum Science Technologies B **9**, 506-509 (1991)

[105] P. Albella, B. Garcia-Cueto, F. González, F. Moreno, P. C. Wu, T. H. Kim, A. Brown, Y. yang, H. O. Everitt, and G. Videen, *Shape Matters: Plasmonic Nanoparticle Shape Enhances Interaction with Dielectric Substrate*, Nano Letters **11**, 3531-3537 (2011)

[106] M. Moskovits, *Surface-Enhanced Raman Spectroscopy: A Brief Retrospective*, Journal of Raman Spectroscopy **36**, 485-496 (2005)

[107] K. Okamoto, B. Lin, K. Imazu, A. Yoshida, K. Toma, M. Toma, and K. Tamada, *Tuning Colors of Silver Nanoparticle Sheets by Multilayered Crystalline Structures on Metal Substrates*, Plasmonics **8**, 581-590 (2013)

[108] A. Apuzzo, M. Fevrier, R. Salas-Montiel, A. Bruyant, A. Chelnokov, G. Lerondel, B. Dagens, and S. Blaize, *Observation of Near-Field Dipolar Interactions Involved in a Metal Nanoparticle Chain Waveguide*, Nano Letters **13**, 1000-1006 (2013)

[109] P. Colomban, *The Use of Metal Nanoparticles to Produce Yellow, Red and Iridescent Colour, from Bronze Age to Present Times in Lustre Pottery and Glass: Solid State Chemistry, Spectroscopy and Nanostructure*, Journal of Nano Research **8**, 109-132 (2009)

[110] J. Homola, S. S. Yee, and G. Gauglitz, *Surface Plasmon Resonance Sensors: Review*, Sensors and Actuators B **54**, 3-15 (1999)

[111] E. Kretschmann and H. Raether, *Radiative Decay of Non-Radiative Surface Plasmons Excited by Light*, Z. Naturforsch **23**, 2135-2136 (1968)

[112] A. Otto, *Excitation of Surface Plasma Waves in Silver by the Method of Frustrated Total Reflection,* Z. Physik **216**, 398-410 (1968)

[113] A. D. Boardman (Ed.), *Electromagnetic Surface Modes*, John Wiley and Sons, (1982)

[114] J. M. Brockman, B. P. Nelson, and R. M. Corn, *Surface Plasmon Resonance Imaging Measurements of Ultrathin Organic Films*, Annual Review of Physics Chemistry **51**, 41-63 (2000)

[115] W. Knoll, *Interfaces and Thin Films as Seen by Bound Electromagnetic Waves*, Annual Review of Physical Chemistry **49**, 569-638 (1998)

[116] H. Knobloch, H. Brunner, A. Leitner, F. Aussenegg, and W. Knoll, *Probing the Evanescent Field of Propagating Plasmon Surface Polaritons by Fluorescence and Raman Spectroscopies*, Journal of Chemical Physics **98**, 10093-10095

[117] M. M. Miller and A. A. Lazarides, *Sensitivity of Metal Nanoparticle Surface Plasmon Resonance to the Dielectric Environment*, Journal of Physical Chemistry B **109**, 21556-21565 (2005)

[118] T. R. Jensen, M. L. Duval, L. Kelly, A. A Lazarides, G. C. Schatz, and R. P. Van Duyne, *Nanosphere Lithography: Effect of the External Dielectric Medium on the Surface*

Plasmon resonance Spectrum of a Periodic Array of Silver Nanoparticles, Journal of Physical Chemistry B **103**, 9846-9853 (1999)

[119] G. Mie, *Contributions to the Optics of Turbid Media, Particularly Colloidal Metal Solutions*, Annal Physics **25**, 377 (1908)

[120] M. Kerker, *The Scattering of Light and Other Electromagnetic Radiation*, Academic: New York (1969)

[121] C. F. Bohren and D. R. Huffman, *Absorption and Scattering of Light by Small Particles*, Wiley interscience: New York (1983)

[122] C. A. Mirkin, R. L. Letsinger, R. C. Mucic, and J. J. Storhoff, *A DNA-Based Method for Rationally Assembling Nanoparticles into Macroscopic Materials*, Nature **382**, 602-609 (1996)

[123] M. Quinten, A. Leitner, J. R. Krenn, and F. R. Aussenegg, *Electromagnetic Energy Transport via Linear Chains of Silver Nanoparticles*, Optics Letters **23**, 1331-1333 (1998)

[124] S. K. Ghosh, S. Nath, S. Kundu, K. Esumi, and T. Pal, *Solvent and Ligand Effects on the Localized Surface Plasmon Resonance (LSPR) of Gold Colloids*, Journal of Physical Chemistry B **108**, 13963-13971 (2004)

[125] U. Kreibig and M. Vollmer, *Optical Properties of Metal Clusters*, Springer: Berlin (1995)

[126] C. A. Mirkin and M. A. Ratner, *Molecular Electronics*, Annual Review of Physical Chemistry **43**, 719-754 (1992)

[127] M. A. Rampi, O. J. A. Schueller, and G. M. Whitesides, *Alkanethiol Self-Assembled Monolayers as the Dielectric of Capacitors with Nanoscale Thickness*, Applied Physics Letters **72** 1781-1783 (1998)

[128] D. L. Klein, R. Roth, A. K. L. Lim, A. P. Alivisatos, and P. L. McEuen, *A Single-Electron Transistor Made from a Cadmium Selenide Nanocrystal*, Nature **389**, 699-701 (1997)

[129] S. K. Ghosh, S. Kundu, M. Mandal, S. Nath, and T. Pal, *Studies on the Evolution of Silver Nanoparticles in Micelle by UV-Phostoactivation*, Journal of Nanoparticle Research **5**, 577-587 (2003)

[130] A. J. Haes, S. L. Zou, G. C. Schatz, and R. P. Van Duyne, *Nanoscale Optical Biosensor: Short Range Distance Dependence of the Localized Surface Plasmon Resonance of Noble Metal Nanoparticles*, Journal of Physical Chemistry B **108**, 6961-6968 (2004)

[131] P. Hanarp, M. Kali, and D. S. Sutherland, *Optical Properties of Short Range Ordered Arrays of Nanometer Gold Disks Prepared by Colloidal Lithography*, Journal of Physical Chemistry B **107**, 5768-5772 (2003)

[132] T. R. Jensen, M. D. Malinsky, C. L. Haynes, and R. P. Van Duyne, *Nanosphere Lithography: Tunable Localized Surface Plasmon Resonance Spectra of Silver Nanoparticles*, Journal of Physical Chemistry B **104**, 10549-10556 (2000)

[133] M. D. Malinsky, K. L. Kelly, G. C. Schatz, and R. P. Van Duyne, *Chain Length Dependence and Sensing Capabilities of the Localized Surface Plasmon Resonance of Silver Nanoparticles Chemically Modified with Alkanethiol Self-Assembled Monolayer*s, Journal of American Chemical Society **123**, 1471-1482

[134] J. J. Mock, D. R. Smith, and S. Schultz, *Local Refractive Index Dependence of Plasmon Resonance Spectra from Individual Nanoparticles*, Nano Letters **3**, 485-491 (2003)

[135] G. Raschke, S. Brogl, A. S. Susha, A. L. Rogach, T. A. Klar, J. Feldmann, B. Fieres, N. Petkov, T. Bein, A. Nichtl, and K. Kurzinger, *Gold Nanoshells Improve Single Nanoparticle Molecular Sensors*, Nano Letters **4**, 1853-1857 (2004)

[136] A. A. Lazarides and G. C. Schatz, *DNA-Linked Metal Nanosphere Materials: Structural Basis for the Optical Properties*, Journal of Physical Chemistry B **104**, 460-467 (2000)

[137] A. A. Lazarides and G. C. Schatz, *DNA-Linked Metal Nanosphere Materials: Fourier-Transform Solutions for the Optical Response*, Journal of Chemical Physics **112**, 2987-2993 (2000)

[138] A. Pal, S. K. Ghosh, K. Esumi, and T. Pal, *Reversible Generation of Gold Nanoparticle Aggregates with Changeable Interparticle Interactions by UV Photoactivation*, Langmuir **20**, 575-578 (2004)

[139] V. A. Markel, V. M. Shalaev, P. Zhang, W. Huynh, L. Tay, T. L. Haslett, and M. Moskovits, *Near-Field Optical Spectroscopy of Individual Surface-Plasmon Modes in Colloid Clusters*, Physical Review B **59**, 10903-10909 (1999)

[140] A. Furstner, *Active Metals: Preparation Characterization Applications*, John Wiley & Sons, New York (1995)

[141] F. Tam, C. Moran, and N. Halas, *Geometrical Parameters Controlling Sensitivity of Nanoshell Plasmon Resonances to Changes in Dielectric Environment*, Journal of Physical Chemistry B **108**, 17290-17294 (2004)

[142] S. Link, M. B. Mohamed, and M. A. El-Sayed, Journal of Physical Chemistry B **103**, 3073-3077 (1999)

[143] M. M. Miller and A. A. Lazarides, *Sensitivity of Metal Nanoparticle Surface Plasmon Resonance to the Dielectric Environment*, Journal of Physical Chemistry B **109**, 21556-21565 (2005)

[144] A. Hilger, N. Cuppers, M. Tenfelde, and U. Kreibig, *Surface and Interface Effects in the Optical Properties of Silver Nanoparticle*s, European Physical Journal **10**, 115-118 (2000)

[145] M. D. Malinsky, K. L. Kelly, G. C. Schatz, and R. P. Van Duyne, *Nanosphere Lithography: Effect of Substrate on the Localized Surface Plasmon Resonance Spectrum of Silver Nanoparticles*, Journal of Physical Chemistry B **105**, 2343-2350 (2001)

[146] P. K. Jain, and M. A. El-Sayed, *Plasmonic Coupling in Noble Metal Nanostructures*, Chemical Physics Letters **487**, 153-164 (2010)

[147] P. K. Jain, X. Huang, I. H. El-Sayed, M. A. El-Sayed, *Review of some Interesting Surface Plasmon Resonance-Enhanced Properties of Noble Metal Nanoparticles and their Applications to Biosystems*, Plasmonics **2**, 107- 118 (2007)

[148] P. K. Jain, W. Huang, M. A. El-Sayed, *On the Universal Scaling Behavior of the Distance Decay of Plasmon Coupling in Metal Nanoparticle Pairs: A Plasmon Ruler Equation*, Nano Letters **7**, 2080-2088 (2007)

[149] L Gunnarsson, T. Rindzevicius, J. Prikulis, B. Kasemo, M. Kall, S. L. Zou, and G. C. Schatz, *Confined Plasmons in Nanofabricated Single Silver particle Pairs: Experimental Observations of Strong Interparticle Interactions*, Journal of Physical Chemistry B **109**, 1079-1087 (2005)

[150] W. Rechberger, A. Hohenau, A. Leitner, J. R. Krenn, B. Lamprecht, F. R. Aussenegg, *Oprtical Properties of Two Interacting Gold Nanoparticles*, Optics Communications **220**, 137- 141 (2003)

[151] J. J. Storhoff, A. A. Lazarides, R. C. Mucic, C. A. Mirkin, R. I. Letsinger, and G. C. Schatz, *What Controls the Optical Properties of DNA-Linked Gold Nanoparticle Assemblies?* Journal of the American Chemical Society **122**, 4640-4650 (2000)

[152] R. Eighanian, J. J. Storhoff, R. C. Mucic, R. L. Letsinger, and C. A. Mirkin, *Selective Colorimetric Detection of Polynucleotides Based on the Distance-Dependent Optical Properties of Gold Nanoparticles*, Science **277**, 1078-1081 (1997)

[153] K. H. Su, Q. H. Wei, X. Zhang, J. J. Mock, D. R. Smith, and S. Schultz, *Interparticle Coupling Effects on Plasmon Resonances of Nanogold Particles*, Nano Letters **3**, 1087-1090 (2003)

[154] P. K. Jain and M. A. El-Sayed, *Surface Plasmon Coupling and its Universal Size Scaling in Metal Nanostructures of Complex Geometry: Elongated Particle Pairs and Nanosphere Trimers*, Journal of Physical Chemistry C **112**, 4954-4960 (2008)

[155] C. D. Bain and G. M. Whitesides, *Attenuation Lengths of Photoelectrons in Hydrocarbon Films*, Journal of Physical Chemistry **93**, 1670-1673 (1989)

[156] A. S. Duwez, *Exploiting Electron Spectroscopies to Probe the Structure and Organization of Self-Assembled Monolayers: A Review*, Journal of Electron Spectroscopy and Related Phenomena **134**, 97-138 (2004)

[157] J. C. Love, L. A. Estroff, J. K. Kriebel, R. G. Nuzzo, and G. M. Whitesides, *Self-Assembled Monolayers of Thiolates on Metals as a Form of Nanotechnology*, Chemical Reviews **105**, 1103-1169 (2005)

[158] M. G. Samant, C. A. Brown, and J. G. Gordon, *Structure of an Ordered Self-Assembled Monolayer of Docosyl Mercaptan on Gold(111) by Surface X-Ray Diffraction,* Langmuir **7**, 437-439 (1991)

[159] S. J. Stranick, P. S. Weiss, A. N. Parikh, and D. L. Allara, *Alternating Current Scanning Tunneling Spectroscopy of Self-Assembled Monolayers on Gold*, Journal of Vacuum Science and Technology A **11**, 739 (1993)

[160] C. F. Quate, *Scanning Probes as a Lithography Tool for Nanostructures*, Surface Science **386**, 259-264 (1997)

[161] J. A. Venables, *Introduction to Surface and Thin Film Processes*, Cambridge University Press, Cambridge, U.K. (2000)

[162] M. Schlesinger, M. Paunovic, Eds., *Modern Electroplating*, John Wiley & Sons, New York (2000)

[163] D. Baudrand, *Electroless Processes*, Plating and Surface Finishing **87**, 42-44 (2000)

[164] M. J. Hostetler, J. J. Stokes, and R. W. Murray, *Infrared Spectroscopy of Three-Dimensional Self-Assembled Monolayers: N-alkanethiolate Monolayers on Gold Cluster Compounds*, Langmuir **12**, 3604-3612 (1996)

[165] J. C. Love, D. B. Wolfe, R. Haasch, M. L. Chabinyc, K. E. Paul, G. M. Whitesides, and R. G. Nuzzo, *Formation and Structure of Self-Assembled Monolayers of Alkanethiolates on Palladium*, Journal of the American Chemical Society **125**, 2597-2609 (2003)

[166] H. O. Finklea, *Electrochemistry of Organized Monolayers of Thiols and Related Molecules on Electrodes*, Electroanalytical Chemistry**19**, 109-335 (1996)

[167] R. Naumann, S. M. Schiller, F. Giess, B. Grohe, K. B. Hartman, I. Karcher, I. Koper, J. Lubben, K. Vasilev, and W. Knoll, *Tethered Lipid Bilayers on Ultraflat Gold Surfaces*, Langmuir **19**, 5435-5443 (2003)

[168] G. Kastle, H. G. Boyen, B. Koslowski, A. Plettl, F. Weigl, and P. Ziemann, *Growth of Thin, Flat Epitaxial (111) Oriented Gold Films on C-Cut Sapphire*, Surface Science **498**, 168-174 (2002)

[169] M. H. Dishner, M. M. Ivey, S. Gorer, J. C. Hemminger, and F. J. Feher, *Preperation of Gold Thin Films by Epitaxial Growth on Mica and the Effect of Flame Annealing*, Journal of Vacuum Science and Technology A **16**, 3295-3300 (1998)

[170] F. Jiang, Y. K. Leong, M. Saunders, M. Martyniuk, L. Faraone, A. Keating, and J. M. Dell, *Uniform Dispersion of Lanthanum Hexaboride Nanoparticles in a Silica Thin Film: Synthesis and Optical Properties*, ACS Applied Materials & Interfaces **4**, 5833-5838 (2012)

[171] R. Zanella, S. Giorgio, C. H. Shin, C. R. Henry, and C. Louis, *Characterization and Reactivity in CO Oxidation of Gold Nanoparticles Supported on TiO_2 Prepared by Deposition-Precipitation with NaOH and Urea*, Journal of Catalysis **222**, 357-367 (2004)

[172] H. Y. Fan, K. Yang, D. M. Boye, T. Sigmon, K. J. Malloy, H. F. Xu, G. P. Lopez, and C. J. Brinker, *Self-Assembly of Ordered, Robust, Three-Dimensional Gold Nanocrsytal/Silica Arrays*, Science **304**, 567-571 (2004)

[173] G. H. Woehrle, M. G. Warner, and J. E. Hutchinson, *Ligand Exchange Reactions Yield Subnanometer, Thiol-Stabilized Gold Particles with Defined Optical Transitions*, Journal of Physical Chemistry B **106**, 9979-9981 (2002)

[174] A. Wijaya and K. Hamad-Schifferli, *Ligand Customization and DNA Functionalization of Gold Nanorods via Round-Trip Phase Transfer Ligand Exchange*, Langmuir **24**, 9966-9969 (2008)

[175] D. H. Chen and C. H. Hsieh, *Synthesis of Nickel Nanoparticles in Aqueous Cationic Surfactant Solution*, Journal of Materials Chemistry **12**, 2412-2415 (2002)

[176] D. H. Dahanayaka, J. X. Wang, S. Hossain, and L. A. Bumm, *Optically Transparent Au{111} Substrates: Flat Gold Nanoparticle Platforms for High-Resolution Scanning Tunneling Microscopy*, Journal of the American Chemical Society **128**, 6052-6053 (2006)

[177] J. Meier, K. A. Friedrich, and U. Stimming, *Novel Method for the Investigation of Single Nanoparticle Reactivity*, Faraday Discussions **121**, 365-372 (2002)

[178] I. Lopez-Salido, D. C. Lim, and Y. D. Kim, *Ag Nanoparticles on Highly Ordered Pyrolytic Graphite (HOPG) Surfaces Studied Using STM and XPS*, Surface Science **588**, 6-18 (2005)